Reduced Order Modeling of Aircraft Structural Assembly using Spectral Finite Element Method

A Dissertation

Submitted in the Partial Fulfillment of the

Requirements for the Degree of Master of Engineering

in Aerospace Engineering

By

K. Sainath

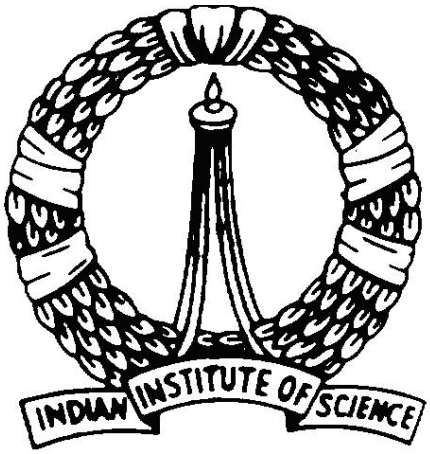

June 2012

Department of Aerospace Engineering

Indian Institute of Science

Bangalore – 560012

Dedicated

To

My Parents

Acknowledgment

I now take the opportunity to express my gratitude to all those who supported me to complete this thesis work.

I express my sincere gratitude to Dr. Debasish Ghose, Chairman of Aerospace Department, Indian Institute of Science, Bangalore, for providing me the opportunity and all academic facilities with lots of support and encouragement and valuable guidance to successfully complete M.E in Aerospace Engineering.

I express my profound thanks to my supervisors Dr. D. Roy.Mahapatra and Dr. S. N. Omkar, Department of Aerospace Engineering, Indian Institute of Science, Bangalore, for there excellent and valuable guidance and encouragement in successful completion of thesis.

I thank the faculty members and of the Aerospace Department staff for their co-operation. I thank all my friends and my batch mates in IISc for their constant support and encouragement.

I am very much thankful to my beloved parents for their encouragement and support in all my efforts. Finally I thank almighty for giving me sound health and mind during my time at IISc.

K. Sainath

Table of contents

List of Figures

Abstract

This thesis presents a reduced order modeling of aircraft wing; a 2D beam-frame model is formed by combining 1D beam elements. The formulation of dynamic stiffness matrix of 2D beam-frame model is performed using Spectral finite element method.

Dynamic response analysis for 1D rod elements, 1D beam elements and 2D frame has been performed using spectral finite element method. Dynamic response analysis for 2D Beam-Frame model of the wing for two different cases is also been performed.

Chapter 1

Introduction

1.1 Introduction

Studies involving the monitoring, detection and arrest of the growth of flaws such as cracks constitute Structural Health Monitoring (SHM). It is a type of inverse problem where in the presence of damage needs to be detected from the known input and the measured output. Small size damage affects only the higher order modes leaving the lower modes unchanged. Effects of damages of smaller dimensions can be captured only at higher frequencies. To assess the presence of small size damage, one needs a mathematical model that can capture the high frequency response of the damaged structure with small problem sizes. Conventional Finite element modeling is not suitable for high frequency analysis. To solve the wave equation exactly the time domain PDE is transformed to frequency domain ODE. Wave propagation [1] based diagnostic tool is suitable for this kind of analysis. Spectral finite element method (SFEM) is the most efficient computational method for wave propagation analysis in structures [2].

Identification of damages in structure under dynamic loading requires efficient numerical model based tools to solve the resulting inverse problem. Often it is possible, as is the case in the present approach, to estimate the location and severity of damage by solving a forward problem. One of such solution to the problem is termed in our previous works as the Damage Force Indicator (DFI) approach.

The extension of the previously reported computational and experimental developments [1, 2] based on the DFI approach is given in [3]. It is essentially concerned with the use of a sophisticated computational model, namely the dynamic stiffness matrix with essential spectral properties and real-time measurement using a sensor-actuator network. It consists of a model-free approach, meaning the model of the damaged structure is not essential, such that a dynamic stiffness of the baseline structure is sufficient to identify the location of damage and its influence on the force transmission characteristics.

In the present work we attempt to address various modeling and computational issues in constructing the base-line structural dynamic model data for complex structures, starting with a 2D frame and then 2D Beam-Frame model with higher geometric complexities. In practical situations, the DFI, which is a measure of the load transmission capacity of the damaged structure, can be

obtained easily from the measurement of dynamic responses at the nodal locations.

In many large-scale engineering problems efficient handling of the discretized computational model becomes essential. Use of a reduced-order model (ROM) derived from finite element (FE) model of the original system is of particular interest in such problems. In computational structural mechanics, applications of ROM is useful in global/local analysis, reanalysis and structural optimization, eigenvalue problem, structural vibration and buckling, sensitivity studies and control parameter design, model update and damage detection. Different non-structural problems related to heat transfer, fluid-structure interaction and other linear and non-linear steady-state boundary value problems have also been analysed using ROMs. A detail review on the above aspects can be found in [19], Woerkom [20] carried out an elaborate survey of order reduction methods for application in flexible spacecraft dynamics. An applications of ROM in high frequency vibration of linear time invariant flexible elastic structures is found in [10].

The computational issue here is to reduce the on-line computational cost as much as possible by taking advantage of the parallelism that exists between off-line model construction and real-time data acquisition from a sensor network.

In the DFI approach, the diagnostic analysis is performed over a chosen frequency band. This means that we do not separate out the steady-state vibration from the propagating waves. This simplifies the tasks of signal generation and processing to a great extent. Also we can take note of the fact that the interacting wavelengths must be in the order of the size of the damages or smaller. This size versus wavelength effect leaves the possibility that the DFI can be computed over many frequency sub-bands in order to identify the damage size.

Identification of the location and size of the damage using acoustic wave have been demonstrated successfully [4-7]. In [4-7] the damage problem is posed as a inverse problem, Here the damage model is generated as a assembly of 1D beam elements and solved for dynamic response characteristics of the damaged model.

For structures with known material properties, geometry and boundary conditions, a practical and reliable prediction based on the spectral analysis can be made by selective use of the excitation/measurement frequency band over the wave dispersion curves. However, these identified parameters alone cannot provide sufficient information for estimating the damage severity, unless a second set of simulation/experiment has to be performed. This task may be difficult due to time constraints in the operation of a SHM system. Therefore, it would always be advantageous if one can use an integrated scheme, where a

numerical model can be directly used to correlate the acoustic sensor signals with the fracture (or any other form of damage) parameters under the in-service loading conditions.

Since it is useful to deal with the frequency spectra obtained from broadband sensors, one can use the DFI or similar frequency domain measures, which can be computed quickly from spectral response at various locations of the structure. From the DFI vector, if it is identified that the damage exists between two sensor locations, then the same set of data can be used to correlate, for example, the Strain Energy Release Rate (SERR) and further details regarding precise location from the arrival time of high frequency signals.

In the design of vehicles, such as automobiles, aircraft, spacecraft, or submarines, it is important to be able to accurately predict dynamic behavior of the structure. With the extremely high cost of building physical prototypes of these vehicles, there is a growing emphasis on analysis of computer models. In this dissertation, Spectral analysis for a reduced order model of structurally complex aircraft wing is undertaken to explore issues associated with frequency response analysis to practical structures. Of primary interest is the trade-off between computational efficiency and accuracy. Comparisons of the dynamic response measured at the tip of the wing for varying joint stiffness of one of the joint is laid out.

Dynamic response analysis tools used by the aerospace industry rely heavily on a linear approach. Commercial finite element codes make a modal frequency response of a complicated structure straightforward, even for large degree-of-freedom systems. However, this approach is not suitable for predicting the response of aircraft structures when they respond to high dynamic loading in a geometrically nonlinear manner. A nonlinear dynamic analysis in physical DoFs is computationally prohibitive, especially for non-deterministic problems involving long simulation times. It is common practice to reduce the system size by modeling just a portion of the structure e.g. instead of performing analysis for the whole aircraft wing, we can do it for a two 2-dimensional models one along the span of the wing and another along the chord wise direction of the wing. In this dissertation our emphasis will be to go for a reduced order model of aircraft wing, a reduction in one dimension. However, with such an approach, important global dynamics are lost because the assumption taken while modeling the reduced order model will not be valid in the practical scenario and also the boundary conditions cannot be accurately modeled in a spectral analysis.

1.2 Research Objectives

The primary purposes for this study are to:

1. Formulate a reduced order model of the aircraft wing which should be amenable to solve for dynamic characteristics of aircraft wing with scope of incorporating structural damage and related simulation.
2. Formulation of dynamic stiffness for the reduced order model of aircraft wing using spectral finite element method.
3. Perform frequency response analysis for the reduced order model of aircraft wing.

1.3 Outline of thesis

Chapter 2 provides background information for the study of aircraft structures with the component wise discretization.

Chapter 3 includes a detailed understanding of formulation for spectral finite element method for 1D elements and 2D frames.

Chapter 4 focuses on the reduced order modeling of aircraft wing and its formulation using spectral finite element method

Chapter 5 discusses the results obtained using the spectral finite element method for 1D elements, 2D frame and also results obtained for beam-frame model of the aircraft wing using the spectral finite element method.

Chapter 6 Provides the summary and benefits of the study.

Chapter 2

Review of Aircraft Structural components in context of SHM

This chapter presents the background information on the aircraft structural design and its components. It also gives an insight of load transfer from one component to other.

2.1 Aircraft structural design and its components

Aircraft structural design is a subset of structural design in general, including ships, land vehicles, bridges, towers, and buildings. All structures must be designed with care because human life often depends on their performance. Structures are subject to one-way and oscillating stresses, the latter giving rise to fatigue. Metal structures are subject to corrosion, and some kinds of corrosion are accelerated in the presence of stress. Aircraft structures are designed with particular attention to weight, for obvious reasons.

The first aircraft had two wings made of light weight wood frames with cloth skins, held apart by wires and struts. The upper wing and the struts provided compression support while the lower wing and the wires supported tension loads.

In the 1920s, metal began to be used for aircraft structure. A metal wing is a box structure with the skins comprising the top and bottom, with front and back formed by I-beams called *spars*, interior fore-aft stiffeners called *ribs*, and in-out stiffeners called *stringers*. In level flight, the lower skin is in tension while the upper skin is in compression. For this reason, this design is referred to as *stressed skin* construction. During turbulence, upper and lower skins can experience both tension and compression. This box structure is able to support the above-mentioned moments, making single wing aircraft possible. The elimination of the struts and wires so dramatically reduced air drag that aircraft were able to fly twice as fast as before with the same engine.

While automobile structures are spot welded and ships are arc welded, bridges, buildings, and aircraft are riveted or bolted together. Rivets are the preferred fastening method in bridges and buildings mainly because such joints provide some structural damping via internal friction in the rivet-hole and plate-plate interfaces. This damping reduces vibrations and oscillations.

Spot welding is practical for automobile bodies. It is fast, repeatable, and strong. Laser welding is sometimes used on long edge-edge joints in auto

subassemblies because the weight of the overlapped regions of conventional joints is saved and such joints are easy for a laser to access via line-of-sight. Arc welding is rarely used in aluminum because the region around such joints reaches a high temperature and this destroys desirable material properties created by prior rolling and heat treatment. Spot welding is also rare in aluminum because the ever-present tough aluminum oxide on the surface prevents good electrical contact.

As a result, rivets and bolts are used exclusively for aircraft structural joints. Rivet and bolt joints in aircraft are the critical element in aircraft integrity. Great care is expended on creating these joints because they are subject to high stresses. The holes are drilled with keen attention to making their axes normal to the skin surface and their diameters correct. In highly stressed regions of the wing, each hole is manually reamed out to pre-stress the region around the hole. Each rivet or bolt is compressed or torque precisely in order to achieve the stress-carrying capability intended by the structural engineers. Rivet diameter and compression are calculated to ensure that the installed rivet not only completely fills the hole but also creates compressive stress in the surrounding material. If there is any possibility that drilling a hole will leave a burr on the back side, this burr must be manually removed because it could puncture the corrosion-resisting paint when the skins are pulled together by the fastener.

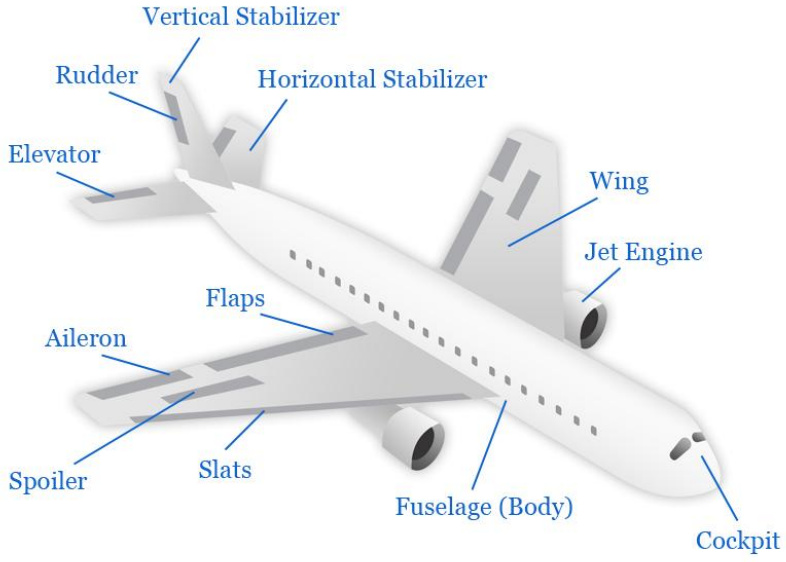

Figure 2-1 Schematic view of Aircraft with its Parts.

Structural engineers take care to choose the size of the fastener to support the stresses it is expected to bear. The same is true of skin thicknesses as mentioned above. On an aircraft wing, the skin may be as much as ten times thicker at the root than it is at the tip. The diameter of fasteners varies similarly, with diameters as large as your thumb at the root and as small as 3 or 4 mm at the tip. Such specialization raises the cost because it reduces economies of scale in purchasing and inventory control, but it saves considerable weight.

The major aircraft structures are wings, fuselage, and empennage. The primary flight control surfaces, located on the wings and empennage, are ailerons, elevators, and rudder. These parts are connected by seams, called joints.

All joints constructed using rivets, bolts, or special fasteners are lap joints. Fasteners cannot be used on joints in which the materials to be joined do not overlap - for example, butt, tee and edge joints.

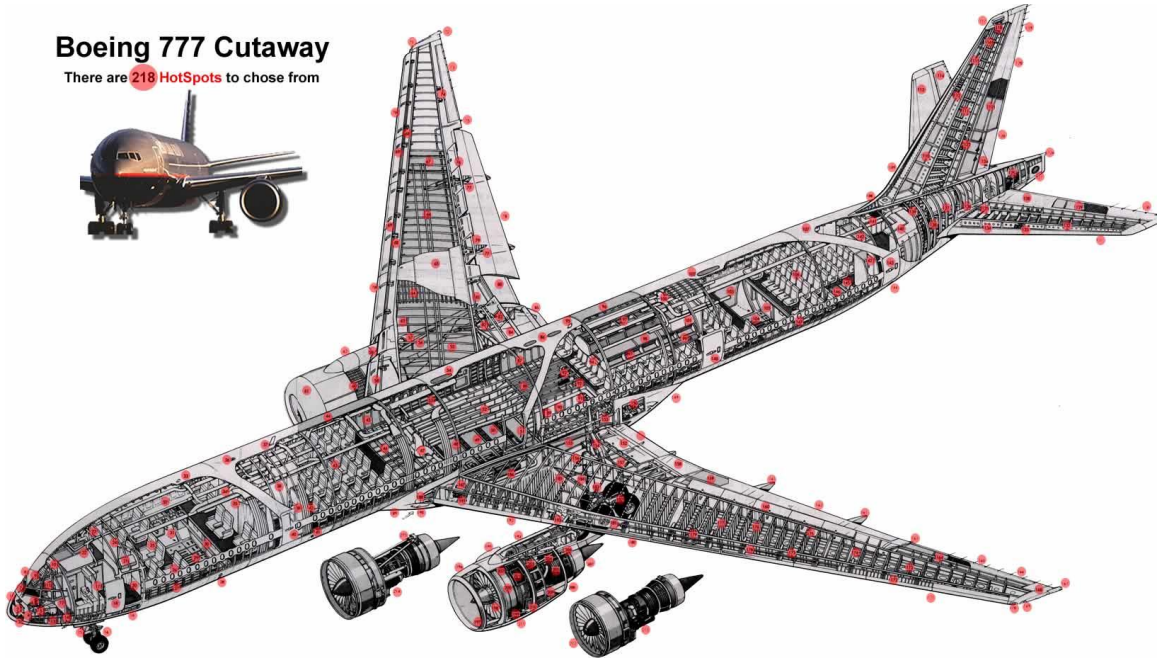

Figure 2-2 Cut-Out View of Boeing 777 Commercial Aircraft.

2.2 Aircraft wings

Aircraft wings have to be strong enough to withstand the positive forces of flight as well as the negative forces of landing. In this dissertation emphasis is

given to metal wings, as the formulation and results produced are confined to metal wings.

Metal wings are of two types: Semi-cantilever and full-cantilever. Semi-cantilever, or braced, wings are used on light aircraft. They are externally supported by struts or flying wires which connect the wing spar to the fuselage. A full cantilever wing is usually made of stronger metal. It requires no external bracing or support. The skin carries part of the wing stress. Parts common to both wing designs are spars, compression ribs, former ribs, stringers, stress plates, gussets, wing tips and wing skins.

2.2.1 Components of the aircraft wing

2.2.1.1 Wing spars

Two or more spars are used in the construction of a wing. They carry the main bending and torsional load from wing root to tip. Both the spar and a compression rib connect the wing to the fuselage.

2.2.1.2 Compression ribs

Compression ribs carry the main load in the direction of flight, from leading edge to trailing edge. On some aircraft the compression rib is a structural piece of tubing separating two main spars. The main function of the compression rib is to absorb the force applied to the spar when the aircraft is in flight.

2.2.1.3 Former ribs

A former rib, which is made from light metal, attaches to the stringers and wing skins to give the wing its aerodynamic shape. Former ribs can be classified as nose ribs, trailing edge ribs, and mid ribs running fore and aft between the front and rear spar on the wing.

2.2.1.4 Stringers

Stringers are made of thin sheets of preformed extruded or hand-formed aluminum alloy. They run front to back along the fuselage and from wing butt to wing tip. Riveting the wing skin to both the stringer and the ribs gives the wing additional strength.

2.2.1.5 Stress plates

Stress plates are used on wings to support the weight of the fuel tank. Some stress plates are made of thick metal and some are of thin metal

corrugated for strength. Stress plates are usually held in place by long rows of machine screws, with self-locking nuts, that thread into specially mounted channels. The stress-plate channeling is riveted to the spars and compression ribs.

2.2.1.6 Gussets

Gussets, or gusset plates, are used on aircraft to join and reinforce intersecting structural members. Gussets are used to transfer stresses from one member to another at the point where the members join.

2.2.1.7 Wing tips

The wing tip, the outboard end of the wing, has two purposes: To aerodynamically smooth out the wing tip air flow and to give the wing a finished look.

2.2.1.8 Wing skins

Wing skins cover the internal parts and provide for a smooth air flow over the surface of the wing. On full cantilever wings, the skins carry stress. However, all wing skins are to be treated as primary structures whether they are on braced or full cantilever surfaces. Wing skin carry shear load coming onto the wing.

2.3 Aircraft fuselage

The largest of the aircraft structural components, there are two types of metal aircraft fuselages: Full monocoque and semimonocoque. The full monocoque fuselage has fewer internal parts and a more highly stressed skin than the semimonocoque fuselage, which uses internal bracing to obtain its strength.

The full monocoque fuselage is generally used on smaller aircraft, because the stressed skin eliminates the need for stringers, former rings, and other types of internal bracing, thus lightening the aircraft structure.

The semimonocoque fuselage drives its strength from the following internal parts: Bulkheads, longerons, keel beams, drag struts, body supports, former rings, and stringers.

2.3.1 Components of the aircraft fuselage

2.3.1.1 Bulkheads

A bulkhead is a structural partition, usually located in the fuselage, which normally runs perpendicular to the keel beam or longerons. A few examples of bulkhead locations are where the wing spars connect into the fuselage, where the cabin pressurization domes are secured to the fuselage structure, and at cockpit passenger or cargo entry doors.

2.3.1.2 Longerons and Keel Beams

Longerons and keel beams perform the same function in an aircraft fuselage. They both carry the bulk of the load traveling fore and aft. The keel beam and longerons, the strongest sections of the aircraft, tie its weight to other aircraft parts, such as power plants, fuel cells, and the landing gears.

2.3.1.3 Drag Struts and Other Fittings

Drag struts and body support fittings are other primary structural members. Drag struts are used on large jet aircraft to tie the wing to the fuselage center section. Body support fittings are used to support the structures which make up bulkhead or floor truss sections.

Former rings and fuselage stringers are not primary structural members. Former rings are used to give shape to the fuselage. Fuselage stringers running fore and aft are used to tie in the bulkheads and former rings.

2.4 Aircraft Empennage Section and primary flight control surfaces

The empennage is the tail section of an aircraft. It consists of a horizontal stabilizer, elevator, vertical stabilizer and rudder. The conventional empennage section contains the same kind of parts used in the construction of a wing. The internal parts of the stabilizers and their flight controls are made with spars, ribs, stringers and skins.

2.4.1 Aircraft empennage components and flight control surfaces

2.4.1.1 Horizontal Stabilizer and Elevator

The horizontal stabilizer is connected to a primary control surface, i.e., the elevator. The elevator causes the nose of the aircraft to pitch up or down. Together, the horizontal stabilizer and elevator provide stability about the

horizontal axis of the aircraft. On some aircraft the horizontal stabilizer is made movable by a screw jack assembly which allows the pilot to trim the aircraft during flight.

2.4.1.2 Vertical Stabilizer and Rudder

The vertical stabilizer is connected to the aft end of the fuselage and gives the aircraft stability about the vertical axis. Connected to the vertical stabilizer is the rudder, the purpose of which is to turn the aircraft about its vertical axis.

2.4.1.3 Ailerons

Elevators and rudders are primary flight controls in the tail section. Ailerons are primary flight controls connected to the wings. Located on the outboard portion of the wing, they allow the aircraft to turn about the longitudinal axis.

When the right aileron is moved upward, the left one goes down, thus causing the aircraft to roll to the right. Because this action creates a tremendous force, the ailerons must be constructed in such a way as to withstand it.

Flight controls other than the three primary ones are needed on high-performance aircraft. On the wings of a wide-body jet, for example, there are as many as thirteen flight controls, including high and low-speed ailerons, flaps, and spoilers.

2.4.1.4 Flaps and Spoilers

Wing flaps increase the lift for take-off and landing. Inboard and outboard flaps on the trailing edge of the wing travel from full up which is neutral aerodynamic flow position to full down causing air to pile up and create lift. Leading edge flaps - Krueger flaps and variable-camber flaps - increase the wing chord size and thus allow the aircraft to take off or land on a shorter runway. Spoilers, located in the center section span-wise, serve two purposes. They assist the high-speed ailerons in turning the aircraft during flight, and they are used to kill the aerodynamic lift during landing by spreading open on touchdown.

2.4.1.5 Trim Tabs

Connected to the primary flight controls are devices called trim tabs. They are used to make fine adjustments to the flight path of an aircraft. Trim tabs are constructed like wings or ailerons, but are considerably smaller.

2.5 Load transfer

The wing and fuselage are the two major components of an aircraft. The horizontal and vertical tails bear close resemblance to the wing. A wing and fuselage structure consists of a collection of basic structural elements. Each component, as a whole, acts like a beam and a torsion member.

In reality, aircraft loads are in the form of air pressure on the skin, concentrated loads from the landing gear, power plants, passenger seats, etc. these loads are to be collected locally and transferred to the major load-carrying members. Without proper care, these loads may produce excessive local deflections that are not permissible from aerodynamic considerations.

2.5.1 Wing structure

The main function of the wing is to pick up the air and power point loads and transmit them to the fuselage. The wing cross-section takes the shape of an airfoil, which is designed based on aerodynamic considerations. The wing as a whole performs the combined function of a beam and a torsion member. It consists of axial members in stringers, bending members in spars and shear panels in the cover skin and webs of the spars.

The spar is a heavy beam running span wise to take transverse shear loads and span wise bending. It is usually composed of a thin shear panel (the web) with a heavy cap or flange at the top and bottom to take bending. Wing ribs are planar structures capable of carrying in-plane loads. They are placed chord wise along the wing span. Besides serving as load distributers, ribs also hold the skin stringer to the designed contour shape. Ribs reduce the effective buckling length of the stringers and thus increase their compressive load capability.

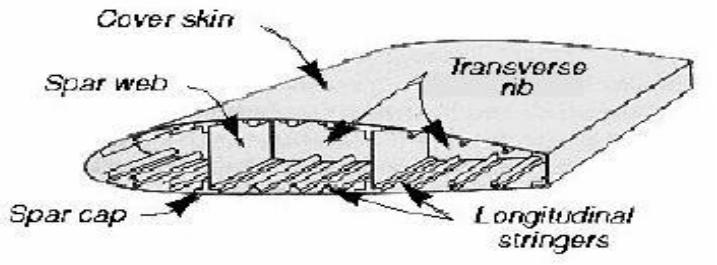

Figure 2-3 Wing Structure

2.5.2 Fuselage

Unlike the wing, which is subjected to large distributed air loads, the fuselage is subjected to relatively small air loads. The primary loads on the fuselage include large concentrated forces from wing reactions, landing gear reactions and payloads. For airplanes with carrying passengers, the fuselage must also withstand internal pressures.

The fuselage structure is a semimonocoque construction consisting of a thin shell stiffened by longitudinal axial elements (stringers and longerons) supported by many transverse frames (bulkheads) along its length. The fuselage skin carries the shear stresses produced by internal pressures. The stringers carry bending moments and axial forces; they also stabilize the thin fuselage skin.Fuselage frames are used to maintain the shape of the fuselage and to shorten the span of the stringers between supports in order to increase the buckling strength of the stringer.

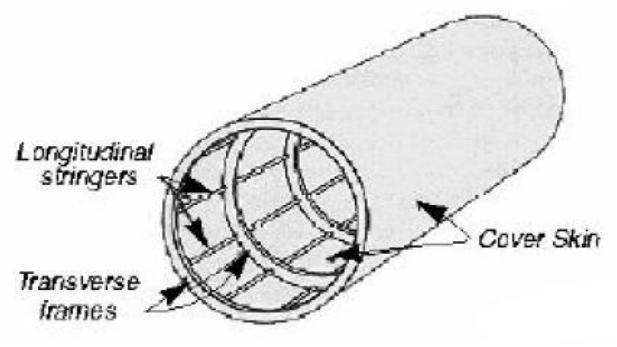

Figure 2-4 Fuselage structure

2.6 Summary

To perform dynamic analysis for aircraft wing, a reduced order model is modeled which is amenable for using spectral finite element method. The components of aircraft wing which are sufficient to capture the dynamic behavior are spars, ribs and skin. Using these parts a reduced order model of the aircraft wing modeled and the formulation of this model is done using spectral finite element method.

Chapter 3

Wave Propagation and Spectral finite element method

This chapter gives an introduction to wave propagation and spectral analysis. It also includes the formulation of 1D elements (rod and beam) using spectral finite element method.

3.1 Wave Propagation

Wave propagation [1] is a transient dynamic phenomenon resulting from short duration impact loads of high frequency content. Impact loads are very often encountered in aircraft structures in the form of gusts, bird hits, tool drops during refurbishment and other transient environments during flight. Structures are an important application Here, the wave propagation studies are used to understand the dynamic behavior of structure subjected to impact loads. Here, the presence of even minute defects and cracks, which occur at initiation of damage and may lead to structural failure, can be detected with help of diagnostic waves. In aircraft structures, the undesired vibration and noise transmit from the source to other parts in the form of wave propagation, and the reduction of this vibration is also another important application of wave propagation studies.

The difference between structural dynamics and wave propagations in structures is the high frequency excitation in the latter problems. If the temporal variation of load is large (of the order of seconds), the frequency content of loading will be low and such problems come under the category of structural dynamics. Since the low frequency load excites only the first few modes, the response of the structure can very well be approximated by the first few normal modes. So the structure can be idealized with fewer degrees of freedom. However, when the duration of the load is of the order of micro to milliseconds, the wave starts propagating in the structure with a finite velocity. So the degrees of freedom required for such models will be many orders higher than structural dynamics problems and they are categorized as wave propagation problems.

In wave propagation, the group velocity of propagation, wave numbers, level of attenuation of the response and the wavelengths are important in the analysis. Therefore, phase information of the waves, which is of no major concern in structural dynamic problems, become really important in wave propagation analysis.

In wave propagation problems, analysis method based on frequency domain is normally used. This is because of the complexities involved in solving the multi-model phenomena problem in the time domain. Here, all the governing equations, boundary conditions and variable are transformed to the frequency domain using Fast Fourier Transforms, which are the numerical implementation of discrete Fourier transforms.

3.2 Spectral Analysis

Spectral analysis is the synthesis of waveforms from the superposition of many frequency components, used to obtain the local behavior of different waveguides and their characteristics. The local behavior is synthesized to obtain the global wave behavior. The phase changes incurred during wave propagation can be expressed using spectral description of waves, by making use of the governing differential for the problem.

In spectral analysis, wave numbers and group speeds are important to understand the wave mechanics in a waveguide. They enable us to know whether the wave mode is propagating or attenuating or a combination of these two. For a propagating wave, the wave numbers will let us understand whether it is dispersive or non-dispersive. If a wave profile changes its shape as it propagates, the wave is said to be dispersive, otherwise it is called non-dispersive.

3.2.1 Waveguide

Any structural element which guides the wave in a definite pattern is a waveguide. Rods are axial or longitudinal waveguides, as they support only axial motion. Beams are called flexural waveguides, as they support only twisting motion. In 2D frames, axial and flexural motions both appear simultaneously and are not coupled with each other.

In general, a waveguide supporting '*n*' different motions will have '*n*' highly coupled governing partial differential equations and hence '*n*' different wave modes, each of which will have unique wave numbers.

3.2.2 Wave number and Spectrum relation

The wave number (*k*) is frequency dependent parameter which determines whether the wave propagates or not, or will propagate after certain frequency. If a wave changes its shape during propagation, it is dispersive wave and if the shape of the wave is retained it is non-dispersive.

If the wave number (*k*) is a linear function of the frequency of the frequency (ω), as k = C ω, (C is constant) then the waves will be non-dispersive in nature, e.g. rods. But if the wave number (*k*) is a non-linear function of the frequency (ω), as $k = C\,\omega^n$, then the waves will be dispersive in nature e.g. in beams and plates. The relation between wave number and frequency is called spectrum relation.

In general, the wave number can be written in complex form as $k = k_R + k_I$, at a given frequency. The real part of the wave number (k_R) represents the propagating wave, while the imaginary part (k_I) represents the spatially decaying damped wave mode.

3.2.3 Phase speed, Group and Dispersion relations

Phase speed (C_P) represents the speed of the individual particles in a wave packet and does not associate with transfer of mass, energy or momentum. If the phase speed is constant and independent of frequency, the wave is non-dispersive in nature. Phase speed is computed as

$$C_p = \left(\frac{\omega}{k_R} \right) \tag{3.1}$$

Group speed (C_g) represents the speed of propagation of a group of waves having same frequency and is associated with the transfer of energy and should be bounded. The time of arrival of all the waves depend on this frequency. If the group speed is constant and independent of frequency, the wave is again non-dispersive in nature.

$$C_g = \left(\frac{d\omega}{dk_R} \right) \tag{3.2}$$

The relation between phase/group speeds and frequency is called dispersion relation and the respective curves are generally called as dispersion curves. For a non-dispersive system, the phase speed and group speed will be same.

3.2.4 Relation between phase speed and group speed

From Eqn. (3.1), we get

$$k_R = \left(\frac{\omega}{C_p} \right) \tag{3.3}$$

Substituting Eqn.(3.3) in Eqn.(3.2), gives the following form as

$$C_g = d\omega \left[d\left(\frac{\omega}{C_p} \right) \right]^{-1} = d\omega \left[\left(\frac{d\omega}{C_p} \right) - \left(\omega \frac{dC_p}{C_p^2} \right) \right]^{-1} = C_p^2 \left[C_p - \left(\omega \frac{dC_p}{d\omega} \right) \right]^{-1} \tag{3.4}$$

From Eqn.(3.4), it is obvious that,

When,

$$\frac{dC_p}{d\omega} = 0, C_g = C_p$$

Also,

$$\frac{dC_p}{d\omega} \Rightarrow \infty, \ cut-off \ \ C_g \Rightarrow 0$$

3.2.5 Cut-off frequency

Cut-off frequency corresponds to the frequency, Here a purely imaginary wave number changes to a purely real or a complex value with a non-zero real part or vice-versa. Physically, it represents the frequency at which a completely damped non-propagating wave-mode transforms to propagating mode or vice-versa.

3.3 Spectral finite Element Method (SFEM)

Spectral finite element method (SFEM) [2], is considered as the most suitable technique for studying wave propagation in structural waveguides subjected to high frequency content loading. For this type of loading, the wave propagation analysis by conventional finite element method (CFEM) is computationally expensive, since the element size should be of the order of wavelength. However in SFEM, the governing equation is transformed first to frequency domain using discrete Fourier transform (DFT). In doing so, the governing partial differential equation (PDE) is reduced to a set of ordinary differential equations (ODE) with constant coefficients, where the time coordinate is removed from the formulation and the frequency is introduced as a parameter. Hence the time doesn't appear explicitly, but is replaced by phase relationships among the field variables which are complex in nature. The resulting ODEs can be solved exactly and the elements are formulated using the exact solution of the governing ODEs as

interpolating functions. The size of the global dynamic stiffness matrix is appreciably smaller than that involved in the CFEM. The steps to be followed in SFEM are as follows:

a) The exact dynamic stiffness is generated and assembled for each sampled frequency and the force-displacement relationship is solved for unit impulse to determine the system transfer function (also called the frequency response function, FRF)
b) The FRF is then convolved with the Fourier coefficient of the load.
c) Next, Inverse fast Fourier transform (IFFT) is used to get the time history of the response.

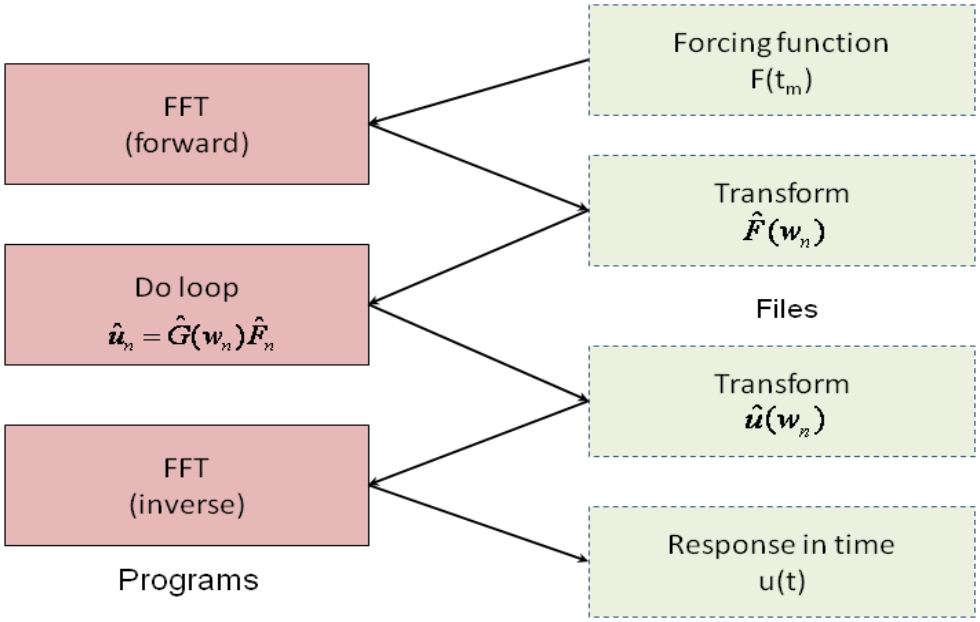

Figure 3-1 Outline of FFT Based Spectral Finite Element Method.

3.4 Spectral Element for Rods

In the aircraft structural assembly the rod like components are stringers in the wing assembly and longerons in the fuselage assembly.

Because the dynamic behavior of a structure is of great importance in engineering, it is necessary to be able to accurately predict the dynamic characteristics of the structure. The finite element method (FEM) has been used extensively in structural dynamics. The finite element model may provide accurate dynamic characteristics of a structure if the wavelength is large compared to the mesh size. However, the finite element solutions become increasingly inaccurate as the frequency increases. Although the accuracy can be improved by refining the mesh, this is sometimes prohibitively expensive in

two- and three-dimensional problems. The conventional finite element (mass and stiffness) matrices are usually formulated from assumed frequency- independent polynomial shape functions. Because the vibrating shape of a structure varies with the frequency of vibration in reality, the FEM requires subdivision of the structure into finite elements (or a mesh) for accurate solutions. Alternatively, if the shape functions are frequency dependent, then the subdivision may not be necessary. This leads to the dynamic stiffness matrix method.

The dynamic stiffness matrix is formulated from the frequency-dependent (or dynamic) shape functions that are exact solutions of the governing differential equations [15]. This frequency-dependent matrix has both mass and stiffness properties of the structural element embedded in it. Because the dynamic stiffness matrix is obtained by directly solving the governing differential equations, all assumptions, being within the limits of the classical theory of differential equations of motion only, are less severe than those made in the FEM and other approximate methods. Thus, the dynamic stiffness matrix method certainly provides more accurate predictions of structural dynamic characteristics. Because the dynamic stiffness matrix method does not require subdivision of a structural member into finite elements, it may eliminate discretization errors and is capable of predicting an infinite number of Eigen solutions by means of a minimum number of degrees of freedom (DOF). This improves the solution accuracy and lowers the computation cost significantly. Because the dynamic stiffness matrix is stiffness formulated, it can be assembled at a specified frequency in a completely analogous way to that used for the FEM. Thus, the assembly feature of the FEM can be equally applied to the dynamic stiffness matrix method.

The dynamic stiffness relation is found via dynamic shape functions, these are essentially interpolation functions between the element ends, but instead of being simple polynomials, they are the exact displacement distributions.

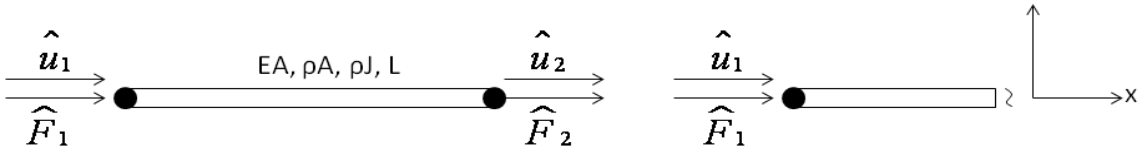

(a) Finite Element **(b) Throw-off Element**

Figure 3-2 Nodal Loads and Degrees of Freedom for Longitudinal Spectral Elements.

3.4.1 Shape functions

Let $\hat{u}$ be the general longitudinal displacement for a rod, $\hat{u}_1$ be the longitudinal displacement at nodal point 1, $\hat{u}_2$ be the longitudinal displacement at nodal point 2 and $\hat{F}(x)$ be the member forces for a rod.

Let k_1 be the wave number for the longitudinal spectral element, $\hat{E}$ be the young's modulus of the rod, $\hat{A}$ be the cross sectional area of the rod and *L* be the length of the rod.

The general longitudinal displacement for a rod is

$$\hat{u}\ x\ = Ae^{-ik_1 x} + Be^{-ik_1(L-x)} \tag{3.5}$$

Here

A, B are constants determined from the boundary conditions on the element.

The displacement end conditions for a finite element, shown in figure 3.2(a), are

$$\hat{u}\ 0\ \equiv \hat{u}_1 = A + Be^{-ik_1 L}, \qquad \hat{u}\ L\ \equiv \hat{u}_2 = Ae^{-ik_1 L} + B \tag{3.6}$$

After solving for *A, B* in terms of the nodal displacements, the longitudinal displacement at an arbitrary point in a finite rod is

$$\hat{u} = \hat{g}_1(x)\hat{u}_1 + \hat{g}_2(x)\hat{u}_2 \tag{3.7}$$

Here

$\hat{g}_1(x)\ and\ \hat{g}_2(x)$ are the frequency-dependent rod shape functions, are given by

$$\hat{g}_1(x) = \frac{[e^{-ik_1 x} - e^{-ik_1(2L-x)}]}{\Delta}$$

$$\hat{g}_1(x) = \frac{[-e^{-ik_1(L+x)} + e^{-ik_1(L-x)}]}{\Delta}\ \text{And}$$

$$\Delta = [1 - e^{-i2k_1 L}]$$

The significance of the shape functions is that the complete description of the element is captured in the two nodal degrees of freedom $\hat{u}_1, \hat{u}_2$. Since the spectral element can be very long, using the shape function and the nodal values response between nodes is computed.

The displacements and the member forces are

$$\hat{u}(x) = \hat{g}_1(x)\hat{u}_1 + \hat{g}_2(x)\hat{u}_2 \tag{3.8}$$

$$\hat{F}(x) = \widehat{EA}[\hat{g}_1'(x)\hat{u}_1 + \hat{g}_2'(x)\hat{u}_2] \tag{3.9}$$

The displacement end conditions for a throw-off element, shown in figure 3.2(b), are

$$\hat{u}(0) = \hat{u}_1$$

The displacement at an arbitrary point for a throw-off element is

$$\hat{u}(x) = \hat{g}_1(x)\hat{u}_1, \qquad \hat{g}_1(x) \equiv [e^{-ik_1x}] \tag{3.10}$$

The shape function $\hat{g}_1(x)$ is frequency dependent and is complex even in simple rod case with no damping.

3.4.2 Dynamic stiffness for rods

The member loads for finite element at each end of the rod are related to the displacements by

$$\hat{F}_1 = -\hat{F}(0) = -\widehat{EA}[\hat{g}_1'(0)\hat{u}_1 + \hat{g}_2'(0)\hat{u}_2] \tag{3.11}$$

$$\hat{F}_2 = +\hat{F}(L) = +\widehat{EA}[\hat{g}_1'(L)\hat{u}_1 + \hat{g}_2'(L)\hat{u}_2] \tag{3.12}$$

Equation (3.11) and (3.12) are written as,

$$\begin{Bmatrix}\hat{F}_1\\ \hat{F}_2\end{Bmatrix} = \widehat{EA}\begin{bmatrix}-\hat{g}_1'(0) & -\hat{g}_2'(0)\\ \hat{g}_1'(L) & \hat{g}_2'(L)\end{bmatrix}\begin{Bmatrix}\hat{u}_1\\ \hat{u}_2\end{Bmatrix} = \begin{bmatrix}\hat{k}_{11} & \hat{k}_{12}\\ \hat{k}_{21} & \hat{k}_{22}\end{bmatrix}\begin{Bmatrix}\hat{u}_1\\ \hat{u}_2\end{Bmatrix} \tag{3.13}$$

Equation (3.13) in short notation is written as,

$$\{\hat{F}\} = [\hat{k}]\{\hat{u}\} \tag{3.14}$$

Here $[\hat{k}]$ is the frequency dependent dynamic element stiffness matrix for the rod, it is symmetric as seen from the explicit matrix form

$$\begin{Bmatrix}\hat{F}_1\\ \hat{F}_2\end{Bmatrix} = \frac{\widehat{EA}}{L}\frac{ik_1L}{(1-e^{-ik_1L})}\begin{bmatrix}1+e^{-ik_1L} & -2e^{-ik_1L}\\ -2e^{-ik_1L} & 1+e^{-ik_1L}\end{bmatrix}\begin{Bmatrix}\hat{u}_1\\ \hat{u}_2\end{Bmatrix} \tag{3.15}$$

The stiffness relation for throw-off element is

$$\{\hat{F}_1\} = \widehat{EA}[i\hat{k}_1]\{\hat{u}_1\} \tag{3.16}$$

Equation (3.15) gives the stiffness relation for finite element and equation (3.16) gives the stiffness relation for throw-off element

3.5 Spectral elements for beams

In the aircraft structural assembly the components which can be approximated as beam elements are spars in the wing assembly. The wing assembly and fuselage assembly separately as a whole resemble their behavior with the beam; they can be approximated as beam elements.

The approach followed here for beams is much the same as in the previous section for rods but since beams are two-mode systems, then there must be two degrees of freedom at each node making the stiffness matrix of order [4×4].

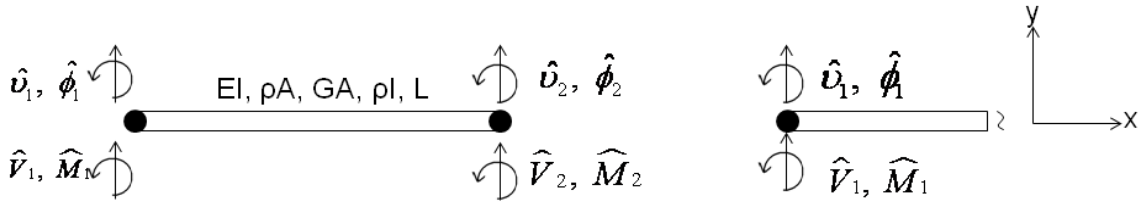

(a) Finite element **(b) Throw-off element**

Figure 3-3 Nodal Loads and Degrees of Freedom for Flexural Spectral elements.

3.5.1 Shape functions

Let $\hat{v}(x)$ be the general transverse displacement, $\hat{\phi}(x)$ be the general transverse rotation degree of freedom for flexural spectral element.

Let k_1, k_2 be the two wave numbers for two-mode system of the flexural spectral element, L is the length of the flexural spectral element.

The general displacement for a Timoshenko beam is

$$\hat{v}(x) = R_1 A e^{-ik_1 x} + R_2 B e^{-ik_2 x} - R_1 C e^{-ik_1 (L-x)} - R_2 D e^{-ik_2 (L-x)} \tag{3.17}$$

$$\hat{\phi}\ x\ = Ae^{-ik_1 x} + Be^{-ik_2 x} + Ce^{-ik_1 (L-x)} + De^{-ik_2 (L-x)} \tag{3.18}$$

Here

A,B,C,D - Coefficients determined from the boundary conditions on the element.

R_i - Amplitude ratios given by

$$R_i = \frac{ik_i GAK_1}{GAK_1 k_i^2 - \rho A \omega^2} \tag{3.19}$$

For throw-off element with C=D=0, the end conditions require that

$$\hat{\upsilon}(0) = \hat{\upsilon}_1 = R_1 A + R_2 B, \quad \hat{\phi}(0) = \hat{\phi}_1 = A + B \tag{3.20}$$

The Coefficients A and B can be re-written in terms of the nodal displacement $\hat{\upsilon}_1$ and rotation $\hat{\phi}_1$.

The displacement can be written as

$$\hat{\upsilon}\ x\ = \hat{g}_{\upsilon 1}\ x\ \hat{\upsilon}_1 + \hat{g}_{\upsilon 2}\ x\ \hat{\phi}_1, \qquad \hat{\phi}\ x\ = \hat{g}_{\phi 1}(x)\hat{\upsilon}_1 + \hat{g}_{\phi 2}(x)\hat{\phi}_1 \tag{3.21}$$

Here

$\hat{g}_i(x)$ are the frequency dependent beam shape functions and are given by

$$\begin{aligned}
\hat{g}_{\upsilon 1}(x) &= [R_1 e^{-ik_1 x} - R_2 e^{-ik_2 x}]/\Delta \\
\hat{g}_{\upsilon 2}(x) &= [-R_1 R_2 e^{-ik_1 x} + R_1 R_2 e^{-ik_2 x}]/\Delta \\
\hat{g}_{\phi 1}(x) &= [e^{-ik_1 x} - e^{-ik_2 x}]/\Delta \\
\hat{g}_{\phi 2}(x) &= [-R_2 e^{-ik_1 x} + R_1 e^{-ik_2 x}]/\Delta
\end{aligned} \tag{3.22}$$

$$\Delta \equiv\ R_1 - R_2$$

The complete description of this element has now been captured in the two nodal degrees of freedom $\hat{\upsilon}_1\ and\ \hat{\phi}_1$.

For a finite element, the end conditions on the element are

$$\hat{\upsilon}(0) = \hat{\upsilon}_1, \quad \hat{\phi}(0) = \hat{\phi}_1, \quad \hat{\upsilon}(L) = \hat{\upsilon}_2, \quad \hat{\phi}(L) = \hat{\phi}_2 \tag{3.23}$$

The displacement solution is

$$\upsilon(x), \phi(x)^{\ T} = \phi_{\ 1} A e^{-ik_1 x} + \phi_{\ 2} B e^{-ik_2 x} + \phi_{\ 3} C e^{-ik_1 (L-x)} + \phi_{\ 4} D e^{-ik_2 (L-x)} \tag{3.24}$$

Here

$\phi_{\ i}$ Are the respective amplitude ratios

Equation (3.24) is written as

$$\upsilon(x), \phi(x)^{\ T} = u\ (x) = [\Phi_A][e(x)]\ A\ + [\Phi_B][e(L-x)]\ B \tag{3.25}$$

Here the two vectors of amplitude are

$$A \equiv \begin{Bmatrix} A \\ B \end{Bmatrix}, \qquad B \equiv \begin{Bmatrix} C \\ D \end{Bmatrix}, \qquad [e(x)] \equiv \begin{bmatrix} e^{-ik_1 x} & 0 \\ 0 & e^{-ik_2 x} \end{bmatrix} \tag{3.26}$$

We have defined the amplitude ratio matrices as

$$[\Phi_A] \equiv \begin{bmatrix} \begin{Bmatrix} \phi_\upsilon \\ \phi_\phi \end{Bmatrix}_1 & \begin{Bmatrix} \phi_\upsilon \\ \phi_\phi \end{Bmatrix}_2 \end{bmatrix}, \qquad [\Phi_B] \equiv \begin{bmatrix} \begin{Bmatrix} \phi_\upsilon \\ \phi_\phi \end{Bmatrix}_3 & \begin{Bmatrix} \phi_\upsilon \\ \phi_\phi \end{Bmatrix}_4 \end{bmatrix} \tag{3.27}$$

The matrix $[\Phi]$is modal matrix. It is fully populated matrix of order [2×2] and typically is not symmetric. The matrix $[e(x)]$is diagonal and is the unit matrix when the argument is zero.

Nodal displacement at x=0 and x=L is written in terms of vectors {A} and {B} as,

$$\begin{Bmatrix} \hat{\upsilon}_1 \\ \hat{\phi}_1 \\ \hat{\upsilon}_2 \\ \hat{\phi}_2 \end{Bmatrix} = \begin{bmatrix} [\Phi_A][e(0)] & -[\Phi_B][e(L)] \\ [\Phi_A][e(L)] & -[\Phi_B][e(0)] \end{bmatrix} \begin{Bmatrix} A \\ B \\ C \\ D \end{Bmatrix} \tag{3.28}$$

Solving this as a system of matrices to get

$$\begin{Bmatrix} A \\ B \\ C \\ D \end{Bmatrix} = [\hat{G}] \begin{Bmatrix} \hat{\upsilon}_1 \\ \hat{\phi}_1 \\ \hat{\upsilon}_2 \\ \hat{\phi}_2 \end{Bmatrix} = [\hat{G}] \ \hat{u} \tag{3.29}$$

The elements of [4×4] matrix $[\hat{G}]$ are

$$\begin{aligned}
&\hat{G}_{11} = +(r_1 + r_2 e_2)/\Delta, \qquad \hat{G}_{12} = -R_2(r_1 - r_2 e_2)/\Delta \\
&\hat{G}_{13} = -(r_2 + r_1 e_2)/\Delta, \qquad \hat{G}_{14} = +R_2(r_1 e_2 - r_2)/\Delta \\
&\hat{G}_{21} = -(r_1 + r_2 e_1)/\Delta, \qquad \hat{G}_{22} = +R_1(r_1 - r_2 e_1)/\Delta \\
&\hat{G}_{23} = +(r_1 e_1 + r_2)/\Delta, \qquad \hat{G}_{24} = -R_1(r_1 e_1 - r_2)/\Delta \\
&\hat{G}_{31} = -\hat{G}_{13}, \hat{G}_{32} = -\hat{G}_{14}, \quad \hat{G}_{33} = -\hat{G}_{11}, \hat{G}_{34} = \hat{G}_{12} \\
&\hat{G}_{41} = -\hat{G}_{23}, \hat{G}_{42} = -\hat{G}_{24}, \quad \hat{G}_{43} = -\hat{G}_{21}, \hat{G}_{44} = \hat{G}_{22}
\end{aligned} \tag{3.30}$$

Here

$$r_1 = (R_1 - R_2)(1 - e_1 e_2), \qquad r_2 = (R_1 + R_2)(e_1 - e_2), \qquad \Delta = r_1^2 - r_2^2 \tag{3.31}$$

and

$$e_1 = e^{-ik_1 L}, \qquad e_2 = e^{-ik_2 L}.$$

Substituting for the coefficients in the assumed displacement field of equation (3.17 and 3.18), the displacements and rotations can now be written in the compact form as

$$\hat{\phi}(x) = \hat{N}^T [\hat{G}]\ \hat{u}\ , \qquad \hat{\upsilon}(x) = \hat{N}^T [\hat{L}_1][\hat{G}]\ \hat{u} \tag{3.32}$$

Here $\hat{N}^T [\hat{G}]$ and $\hat{N}^T [\hat{L}_1][\hat{G}]$ give the shape functions for $\hat{\phi}(x)$ and $\hat{\upsilon}(x)$, respectively. The {4×1} vector $\hat{N}$ is a function of x given by

$$\hat{N}^T = e^{-ik_1 L} \quad e^{-ik_2 L} \quad e^{-ik_1 (L-x)} \quad e^{-ik_2 (L-x)} \tag{3.33}$$

While the matrix $[\hat{L}_1]$ is diagonal and contain the amplitude ratios

$$[\hat{L}_1] = diag[+R_1, +R_2, -R_1, -R_2] \tag{3.34}$$

3.5.2 Dynamic stiffness for beams

The stiffness relation for the beam element is established by taking appropriate space derivatives of the shape function.

For the throw-off element,

$$\hat{\upsilon}(x) = \hat{g}_{\upsilon 1}(x)\hat{\upsilon}_1 + \hat{g}_{\upsilon 2}(x)\hat{\phi}_1, \qquad \hat{\phi}(x) = \hat{g}_{\phi 1}(x)\hat{\upsilon}_1 + \hat{g}_{\phi 2}(x)\hat{\phi}_1 \tag{3.35}$$

The nodal loads are expressed in terms of the displacement degrees of freedom through the relationships for the structural resultants

$$\hat{M}(x) = +EI\frac{d\hat{\phi}}{dx}, \qquad \hat{V}(x) = -EI\frac{d^2\hat{\phi}}{dx^2} - \rho I\omega^2\hat{\phi} \tag{3.36}$$

Evaluation of these at x=0 leads to the dynamic stiffness as

$$\begin{Bmatrix} -\hat{V}(0) \\ -\hat{M}(0) \end{Bmatrix} = \begin{Bmatrix} \hat{V}_1 \\ \hat{M}_1 \end{Bmatrix} = EI \begin{bmatrix} \hat{k}_{11} & \hat{k}_{12} \\ \hat{k}_{21} & \hat{k}_{22} \end{bmatrix} \begin{Bmatrix} \hat{\upsilon}_1 \\ \hat{\phi}_1 \end{Bmatrix} \tag{3.37}$$

Here the individual stiffness terms are

$$\hat{k}_{11} = \frac{k_2^2 - k_1^2}{R_1 - R_2}, \hat{k}_{12} = \hat{k}_{21} = \frac{i(k_1 - k_2)}{R_1 - R_2}, \hat{k}_{22} = \frac{i(R_1 k_1 - R_2 k_2)}{R_1 - R_2} \tag{3.38}$$

This symmetric throw-off stiffness matrix is complex and therefore the structural stiffness matrix will also be complex after assembling.

The finite element looks the same as the conventional element except that the mass is distributed instead of concentrated at the ends. It is assumed that there are no applied loads between the ends.

Considering a beam waveguide of finite length L with loads applied only at the ends. The shape functions are

$$\hat{\phi}(x) = \hat{N}^T [\hat{G}]\ \hat{u}\ , \qquad \hat{\upsilon}(x) = \hat{N}^T [\hat{L}_1][\hat{G}]\ \hat{u} \tag{3.40}$$

Here

$\hat{u}$ is the collection of four degrees of freedom, This leads to the moments and shear expressions.

$$\begin{aligned} \hat{M}(x) &= +EI\ \hat{N}'^T [\hat{G}]\ \hat{u} \\ \hat{V}(x) &= -EI\ \hat{N}''^T [\hat{G}]\ \hat{u}\ - \rho I \omega^2\ \hat{N}^T [\hat{L}_1][\hat{G}]\ \hat{u} \end{aligned} \tag{3.41}$$

Here primes indicate differentiation. At x=0 and x=L equation (3.41) gives,

$$\begin{Bmatrix} -\hat{V}(0) \\ -\hat{M}(0) \\ -\hat{V}(L) \\ +\hat{M}(L) \end{Bmatrix} = [\partial \hat{N}][\hat{G}] \begin{Bmatrix} \hat{\upsilon}_1 \\ \hat{\phi}_1 \\ \hat{\upsilon}_2 \\ \hat{\phi}_2 \end{Bmatrix} \tag{3.42}$$

Here the square matrix $[\partial \hat{N}]$ contains the derivatives

$$[\partial \hat{N}] = \begin{bmatrix} +EI\ \hat{N}''(0)^T + \rho I \omega^2\ \hat{N}(0)^T [\hat{L}_1] \\ EI\ \hat{N}'(0)^T \\ -EI\ \hat{N}''(L)^T - \rho I \omega^2\ \hat{N}(0)^T [\hat{L}_1] \\ +EI\ \hat{N}'(L)^T \end{bmatrix} \tag{3.43}$$

The relation between the loads and degrees of freedom is

$$\hat{F} = [\hat{k}]\ \hat{u} \tag{3.44}$$

Here

$[\hat{k}]$ - Dynamic stiffness matrix,

$\hat{F}$ - Nodal load Vector with components $\hat{V}_1 \quad \hat{M}_1 \quad \hat{V}_2 \quad \hat{M}_2$, and

$\hat{u}$ - Nodal displacement vector with components $\hat{\upsilon}_1 \quad \hat{\phi}_1 \quad \hat{\upsilon}_2 \quad \hat{\phi}_2$

The individual stiffness terms of the matrix $[\hat{k}]$ are:

$$\begin{aligned}
&\hat{k}_{11} = (k_2^2 - k_1^2)(r_1 z_{22} + r_2 z_{21}) / \Delta, \\
&\hat{k}_{13} = (k_1^2 - k_2^2)(r_1 z_{21} + r_2 z_{22}) / \Delta, \\
&\hat{k}_{12} = [-ik_2(r_1 z_{11} + r_2 z_{12}) + ik_1(r_1 z_{11} + r_2 z_{12}) / \Delta, \\
&\hat{k}_{14} = [-ik_1(r_1 z_{12} + r_2 z_{11}) - ik_2(r_1 z_{12} + r_2 z_{11}) / \Delta, \\
&\hat{k}_{22} = (-ik_1 R_2 + ik_2 R_1)(r_1 z_{22} - r_2 z_{21}) / \Delta, \\
&\hat{k}_{24} = (ik_1 R_2 - ik_2 R_1)(r_1 z_{21} - r_2 z_{22}) / \Delta, \\
&\hat{k}_{23} = -\hat{k}_{14}, \quad \hat{k}_{33} = \hat{k}_{11}, \quad \hat{k}_{34} = -\hat{k}_{12}, \quad \hat{k}_{24} = \hat{k}_{22}.
\end{aligned} \tag{3.45}$$

Here

$$\begin{aligned}
&r_1 = (R_1 - R_2) z_{11}, \\
&r_2 = (R_1 + R_2) z_{12}, \\
&\Delta = (r_1^2 - r_2^2) / EI, \\
&z_{11} = 1 - e^{-ik_1 L} e^{-ik_2 L}, \\
&z_{12} = e^{-ik_1 L} - e^{-ik_2 L}, \\
&z_{22} = 1 + e^{-ik_1 L} e^{-ik_2 L}, \\
&z_{12} = e^{-ik_1 L} + e^{-ik_2 L}.
\end{aligned} \tag{3.46}$$

And the remaining terms are obtained using symmetry.

3.6 Spectral element for 2D frames

The 2D frames are the combination of 1-D beam elements connected together, when beams are part of connected structures they additionally support axial loads. As the transverse displacement and axial displacement are not coupled with each other, the stiffness matrix for a 2D frame is taken as addition of rod stiffness matrix and beam stiffness matrix. This gives the effect of connected structures using 1D beam elements.

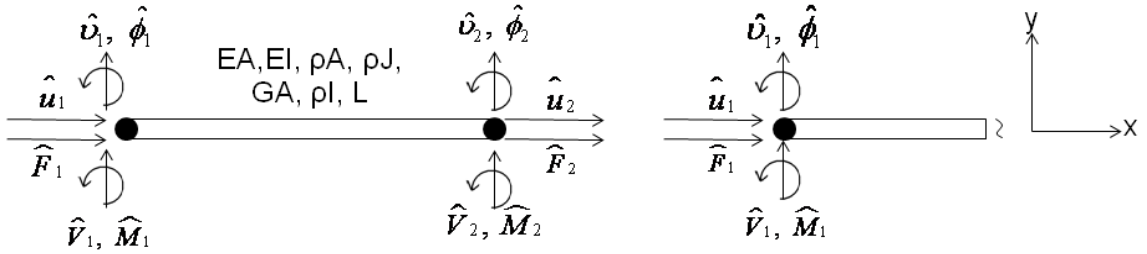

(a) Finite element (b) Throw-off element

Figure 3-4 Nodal loads and degrees of freedom for spectral element of 2D frame

Therefore the stiffness matrix for elements of 2D frames is of dimension [6×6], here the active degrees of freedom are axial displacement, transverse displacement and rotation per node.

3.7 Summary

This chapter has briefly discussed about the construction of the dynamic stiffness matrix for 1D rod, 1D beams and 2D frames.

Chapter 4

Reduced Order Modeling of Aircraft Wing

This chapter covers the reduced order modeling of aircraft wing from a three-dimensional model to a two-dimensional beam-frame model which is amenable for frequency response analysis using spectral finite element method.

4.1 Major Components of Aircraft Wing

The major components of aircraft wing are spars, ribs and skin. To capture the response at the joint of these structures, we take into account of the rivet connections. Here the rivet modeling is not done; instead the effective stiffness of the rivet is added at the respective joint nodes.

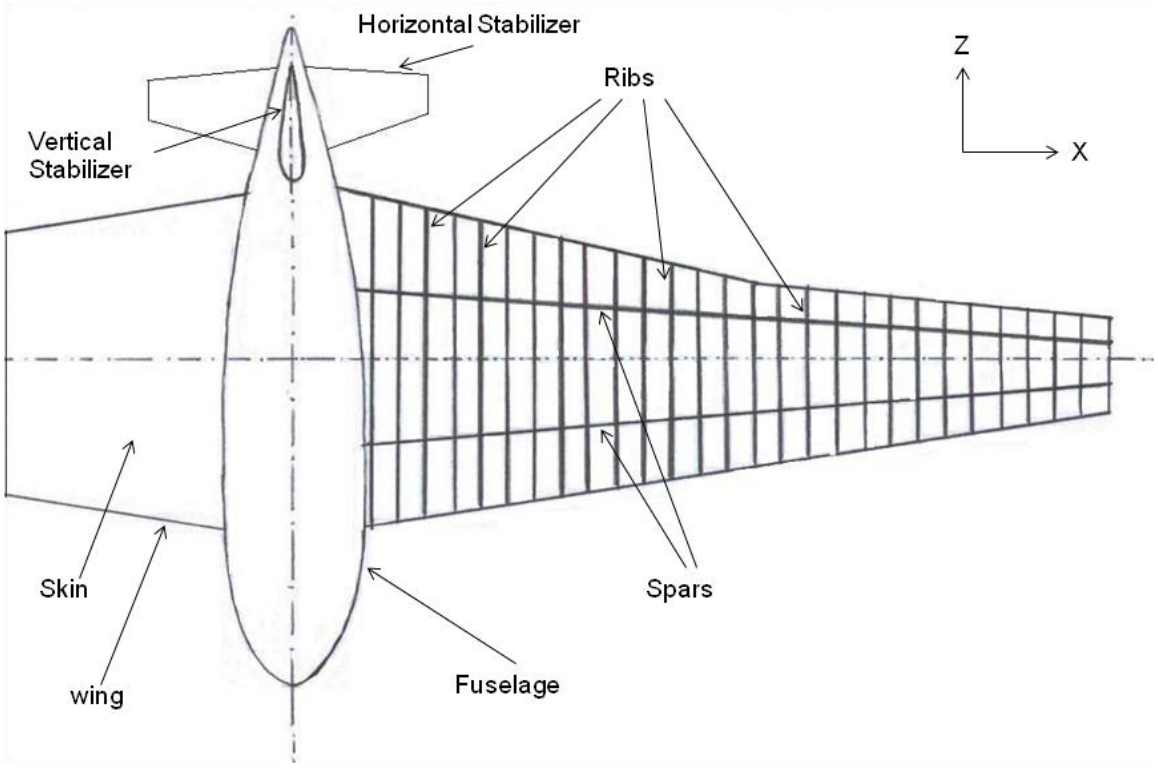

Figure 4-1 Schematic Top View of Aircraft.

The above figure illustrates top sectional view of the aircraft with attention given to wing showing its major components spars, ribs and skin, right wing being un-skinned showing spars running along the span-wise direction, ribs placed along the chord-wise direction and its left wing being skinned.

4.2 Equivalent 2D Beam-Frame Model of an Aircraft Wing

Task is to capture the dynamic characteristics of aircraft wing. It has been discussed that to model the three dimensional wing and perform analysis is too expensive. So, here an equivalent two-dimensional beam-frame model of the aircraft wing is modeled which will be amenable to solve for frequency response analysis using spectral finite element method.

Instead of modeling whole aircraft wing a 2D model of the wing along its span wise direction have modeled, which is capable to capture transverse displacement accurately. The components which have to be taken into account while a reduced order model of the wing is being modeled are spars, ribs and skin.

In the aircraft wing, the spars bear the bending and torsional loads over the wing. The ribs bear the in-plane transverse loads over the wing. The wing skins bear the shear load over the wing.

Here is the schematic view of the aircraft wing in the reduced model as a two-dimensional beam-frame model which is joined to fuselage at one end and free at the other end.

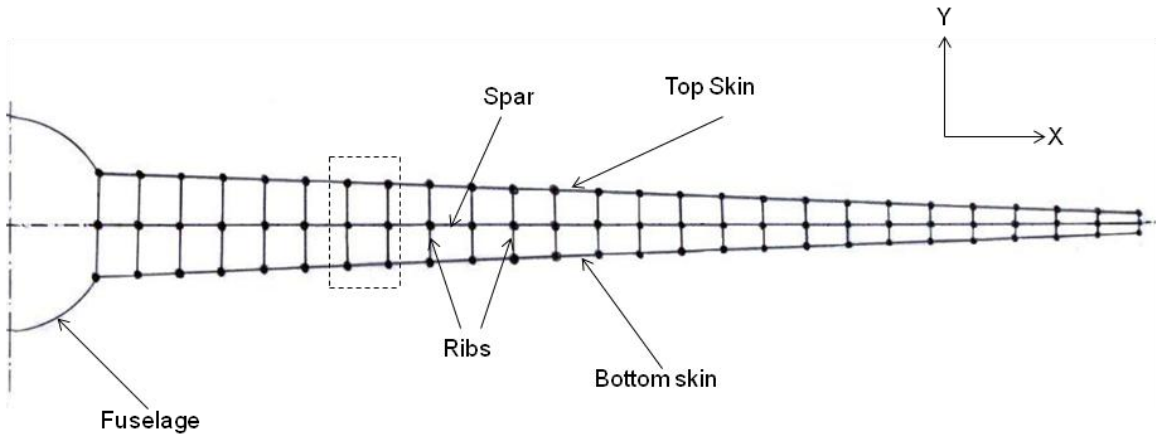

Figure 4-2 Schematic Front View of Reduced order model of Aircraft Wing.

In the above figure the elements which are in the centre from wing root to tip are replaced by spars, the two series of elements above and below the spar elements are replaced by top and bottom skin respectively and the elements normal to spar elements are replaced by ribs (each rib is modeled as a combination of two elements).

The aircraft wing is taken as a stiffened structure, using three of its major components and rivets used to join them. To capture the dynamic characteristics accurately the rivet connections are taken into account, which are used to join ribs to the skin. These rivets are running from leading edge to trailing edge of the wing joining the top and bottom skin with the ribs. The each line of rivets from leading edge to trailing edge of the wing has taken as one rivet line connection, the above connection is valid for the three dimensional wing but when it comes to the reduced order model they have only two nodes. The rivet line connection is replaced with a single distributed spring between these nodes.

The distributed spring is a combination of three springs one each in longitudinal, transverse and rotational directions.

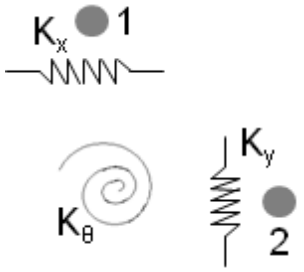

Figure 4-3 Distributed Spring Between node-1 and node-2.

Here

K_x – Stiffness of the spring along longitudinal direction,

K_y – Stiffness of the spring along transverse direction, and

K_θ – Stiffness of the spring along rotational direction.

4.3 Segments of the 2D Beam-Frame Model

To get the dynamic stiffness matrix for the whole 2D beam-frame model is difficult, so the whole model is consider has an assemblage of segments. The part of the model shown in figure 4-4 is a segment between two consecutive ribs.

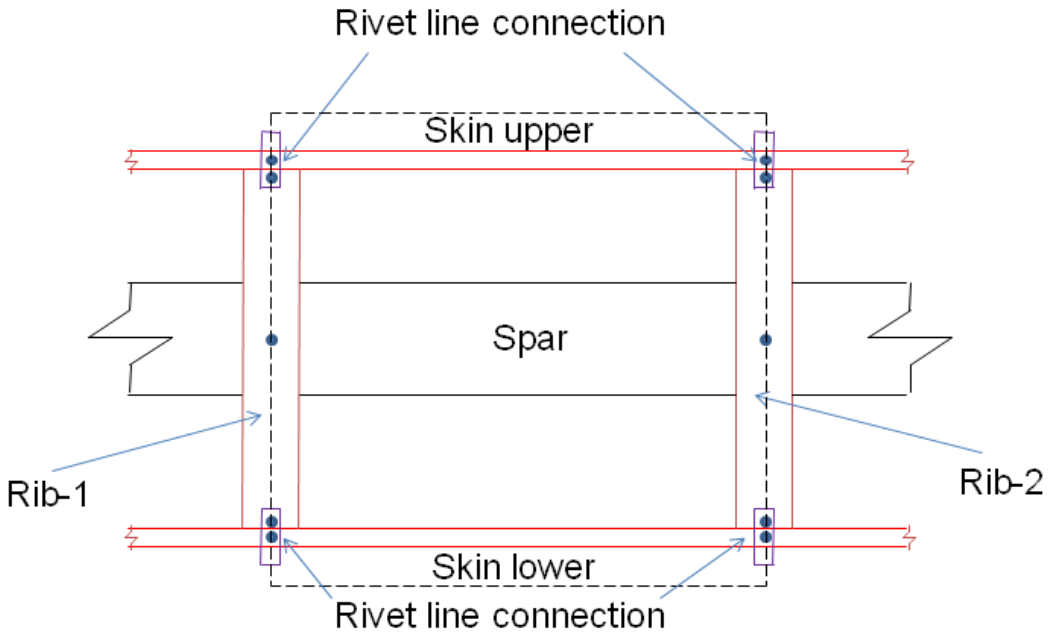

Figure 4-4 2D Beam-Frame model of a Segment of the wing.

Figure 4-5 shows the zoomed view of the segment of beam-frame model. Considering the beam-frame model of one segment formed with seven elements, fourteen distinct nodes and also four distributed springs at the respective joints.

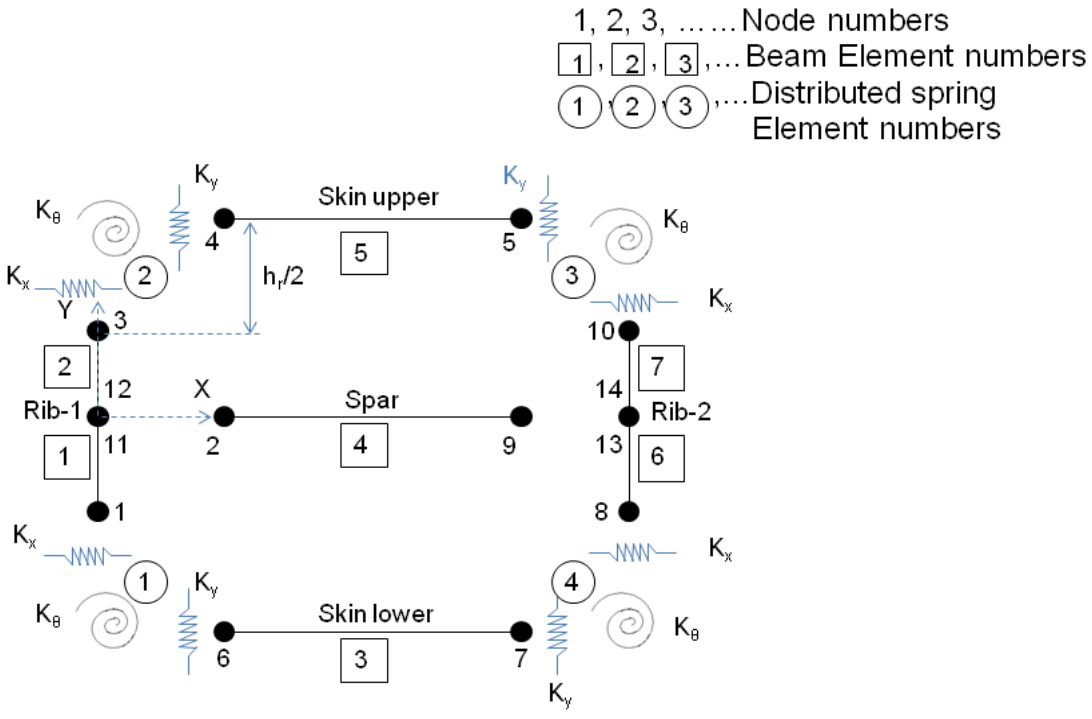

Figure 4-5 A Zoomed-in View of 2D Beam-Frame model of one segment of the wing.

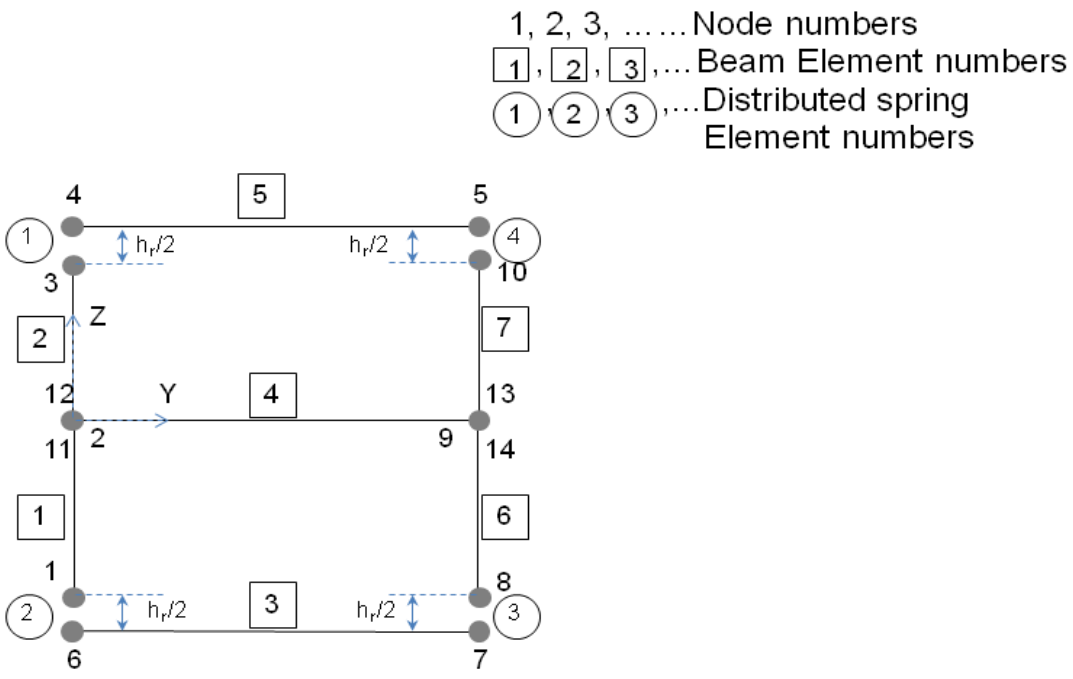

Figure 4-6 One Segment of the 2D Beam-Frame model of the Aircraft Wing.

Figure 4-6 shows the 2D beam-frame model of one segment which goes into the beam-frame model of the wing.

4.4 Formulation of dynamic stiffness matrix of one segment of 2D beam-frame model

The main objective is to get global dynamic stiffness matrix of one segment of 2D beam-frame model using spectral finite element method. Figure 4-5 shows that there are seven elements in the model, which has modeled with 1D beam elements, whose local stiffness matrix is similar to the elements of 2D frame with three active degrees of freedom at each node.

The stiffness matrix for all the seven elements having three degrees of freedom at each node can be assembled together to get the global stiffness matrix. After assembling these elements there is no connectivity between some nodes. This model without the distributed spring does not satisfy compatibility condition; also the global stiffness matrix will be singular.

The stiffness matrix due to the distributed spring is defined as follows.

Let a_r – Area of the single rivet among the rivet line connection on the wing,

d_s – Shank diameter of the rivet,

$n-$ Numbers of rivets along the each rivet line connection,

A_r- Effective area of the distributed spring in reduced order model,

E_r- Young's modulus of the rivet material

G_r- Shear modulus of the rivet material and

h_r- Length of the rivet

Then

$$A_r = n \times a_r \tag{4.1}$$

$$a_r = \frac{\Pi d_s^2}{4} \tag{4.2}$$

Effective stiffness of the distributed spring is defined as,

$$\hat{K}^* = \begin{bmatrix} K_x & 0 & 0 \\ 0 & K_y & 0 \\ 0 & 0 & K_\theta \end{bmatrix} \tag{4.3}$$

Here

K_x- Stiffness of the spring along longitudinal direction,

K_y- Stiffness of the spring along transverse direction, and

$K_\theta-$ Stiffness of the spring along rotational direction.

Considering each spring as an element the stiffness along longitudinal, transverse and rotational direction are as follows

$$K_x = \frac{G_r A_r}{h_r} = \frac{G_r n a_r}{h_r} \tag{4.4}$$

$$K_y = \frac{E_r A_r}{h_r} = \frac{E_r n a_r}{h_r} \tag{4.5}$$

$$K_\theta = \frac{M}{\theta} = \frac{K_y h_r}{\frac{1}{h_r}} = K_y h_r^2 = E_r n a_r h_r \tag{4.6}$$

The stiffness due to distributed spring is dependent on material properties of rivet, no. of rivets in the rivet-line connection, length of the rivet and shank diameter.

From the figure 4-6, Effective stiffness of the distributed spring between node 1 and 6 is given by,

$$\hat{K}_1^* = \begin{bmatrix} K_x^{(1)} & 0 & 0 \\ 0 & K_y^{(1)} & 0 \\ 0 & 0 & K_\theta^{(1)} \end{bmatrix} \tag{4.7}$$

Similarly between node 3 and 4,

$$\hat{K}_2^* = \begin{bmatrix} K_x^{(2)} & 0 & 0 \\ 0 & K_y^{(2)} & 0 \\ 0 & 0 & K_\theta^{(2)} \end{bmatrix} \tag{4.8}$$

Similarly between node 5 and 10,

$$\hat{K}_3^* = \begin{bmatrix} K_x^{(3)} & 0 & 0 \\ 0 & K_y^{(3)} & 0 \\ 0 & 0 & K_\theta^{(3)} \end{bmatrix} \tag{4.9}$$

Similarly between node 7 and 8

$$\hat{K}_4^* = \begin{bmatrix} K_x^{(4)} & 0 & 0 \\ 0 & K_y^{(4)} & 0 \\ 0 & 0 & K_\theta^{(4)} \end{bmatrix} \tag{4.10}$$

Considering the distributed spring between node 1 and 6, from the equilibrium of nodal forces and moments at node 1

$$\begin{aligned} \sum F_X &= \hat{N}_1 + K_X(\hat{u}_1^0 - \hat{u}_6^0) \\ \sum F_Y &= \hat{V}_1 + K_Y(\hat{v}_1 - \hat{v}_6) \\ \sum M &= \hat{M}_1 + K_\varphi(\hat{\varphi}_1 - \hat{\varphi}_6) \end{aligned} \tag{4.11}$$

The above equations in matrix notation can be written as

$$\begin{Bmatrix} \hat{N}_1 \\ \hat{V}_1 \\ \hat{M}_1 \end{Bmatrix} + \begin{bmatrix} K_X & 0 & 0 \\ 0 & K_Y & 0 \\ 0 & 0 & K_\varphi \end{bmatrix} \begin{Bmatrix} \hat{u}_1^0 - \hat{u}_6^0 \\ \hat{v}_1 - \hat{v}_6 \\ \hat{\varphi}_1 - \hat{\varphi}_6 \end{Bmatrix} \tag{4.12}$$

$$\hat{f}_1 + \hat{K}^*(\hat{u}_1 - \hat{u}_6) \tag{4.13}$$

From the equilibrium of nodal forces and moments at node 6

$$\hat{f}_6 + \hat{K}^*(\hat{u}_6 - \hat{u}_1) \tag{4.14}$$

Similarly,

Considering the distributed spring between node 3 and 4

From the equilibrium of nodal forces and moments at node 3

$$\hat{f}_3 + \hat{K}^*(\hat{u}_3 - \hat{u}_4) \tag{4.15}$$

From the equilibrium of nodal forces and moments at node 4

$$\hat{f}_4 + \hat{K}^*(\hat{u}_4 - \hat{u}_3) \tag{4.16}$$

Considering the distributed spring between node 5 and 10

From the equilibrium of nodal forces and moments at node 5

$$\hat{f}_5 + \hat{K}^*(\hat{u}_5 - \hat{u}_{10}) \tag{4.17}$$

From the equilibrium of nodal forces and moments at node 10

$$\hat{f}_{10} + \hat{K}^*(\hat{u}_{10} - \hat{u}_5) \tag{4.18}$$

Considering the distributed spring between node 7 and 8

From the equilibrium of nodal forces and moments at node 7

$$\hat{f}_7 + \hat{K}^*(\hat{u}_7 - \hat{u}_8) \tag{4.19}$$

From the equilibrium of nodal forces and moments at node 8

$$\hat{f}_8 + \hat{K}^*(\hat{u}_8 - \hat{u}_7) \tag{4.20}$$

Considering the dynamic stiffness matrix of element wise waveguide of 2D beam-frame model as follows,

For element (1)

$$\begin{bmatrix} \hat{K}_{11}^{(1)} & \hat{K}_{12}^{(1)} \\ \hat{K}_{21}^{(1)} & \hat{K}_{22}^{(1)} \end{bmatrix} \begin{Bmatrix} \hat{u}_1 \\ \hat{u}_2 \end{Bmatrix} = \begin{Bmatrix} \hat{f}_1 \\ \hat{f}_{11} \end{Bmatrix} \tag{4.21}$$

For element (2)

$$\begin{bmatrix} \hat{K}_{11}^{(2)} & \hat{K}_{12}^{(2)} \\ \hat{K}_{21}^{(2)} & \hat{K}_{22}^{(2)} \end{bmatrix} \begin{Bmatrix} \hat{u}_2 \\ \hat{u}_3 \end{Bmatrix} = \begin{Bmatrix} \hat{f}_{12} \\ \hat{f}_3 \end{Bmatrix} \tag{4.22}$$

For element (3)

$$\begin{bmatrix} \hat{K}_{11}^{(3)} & \hat{K}_{12}^{(3)} \\ \hat{K}_{21}^{(3)} & \hat{K}_{22}^{(3)} \end{bmatrix} \begin{Bmatrix} \hat{u}_6 \\ \hat{u}_7 \end{Bmatrix} = \begin{Bmatrix} \hat{f}_6 \\ \hat{f}_7 \end{Bmatrix} \tag{4.23}$$

For element (4)

$$\begin{bmatrix} \hat{K}_{11}^{(4)} & \hat{K}_{12}^{(4)} \\ \hat{K}_{21}^{(4)} & \hat{K}_{22}^{(4)} \end{bmatrix} \begin{Bmatrix} \hat{u}_2 \\ \hat{u}_9 \end{Bmatrix} = \begin{Bmatrix} \hat{f}_2 \\ \hat{f}_9 \end{Bmatrix} \tag{4.24}$$

For element (5)

$$\begin{bmatrix} \hat{K}_{11}^{(1)} & \hat{K}_{12}^{(1)} \\ \hat{K}_{21}^{(1)} & \hat{K}_{22}^{(1)} \end{bmatrix} \begin{Bmatrix} \hat{u}_4 \\ \hat{u}_5 \end{Bmatrix} = \begin{Bmatrix} \hat{f}_4 \\ \hat{f}_5 \end{Bmatrix} \tag{4.25}$$

For element (6) and

$$\begin{bmatrix} \hat{K}_{11}^{(2)} & \hat{K}_{12}^{(2)} \\ \hat{K}_{21}^{(2)} & \hat{K}_{22}^{(2)} \end{bmatrix} \begin{Bmatrix} \hat{u}_8 \\ \hat{u}_9 \end{Bmatrix} = \begin{Bmatrix} \hat{f}_8 \\ \hat{f}_{13} \end{Bmatrix} \tag{4.26}$$

For element (7)

$$\begin{bmatrix} \hat{K}_{11}^{(3)} & \hat{K}_{12}^{(3)} \\ \hat{K}_{21}^{(3)} & \hat{K}_{22}^{(3)} \end{bmatrix} \begin{Bmatrix} \hat{u}_9 \\ \hat{u}_{10} \end{Bmatrix} = \begin{Bmatrix} \hat{f}_{14} \\ \hat{f}_{10} \end{Bmatrix} \tag{4.27}$$

After assembling wave guide elements and including the effect of the distributed springs through the equilibrium equations the global dynamic stiffness matrix of one segment of the 2D beam-frame model is,

$$\begin{bmatrix} K_{11} & K_{12} & 0 & 0 & 0 & 0 & 0 & 0 & 0 & 0 \\ K_{21} & K_{22} & K_{23} & 0 & 0 & 0 & 0 & 0 & K_{29} & 0 \\ 0 & K_{32} & K_{33} & 0 & 0 & 0 & 0 & 0 & 0 & 0 \\ 0 & 0 & 0 & K_{44} & K_{45} & 0 & 0 & 0 & 0 & 0 \\ 0 & 0 & 0 & K_{54} & K_{55} & 0 & 0 & 0 & 0 & 0 \\ 0 & 0 & 0 & 0 & 0 & K_{66} & K_{67} & 0 & 0 & 0 \\ 0 & 0 & 0 & 0 & 0 & K_{76} & K_{77} & 0 & 0 & 0 \\ 0 & 0 & 0 & 0 & 0 & 0 & 0 & K_{88} & K_{89} & 0 \\ 0 & K_{92} & 0 & 0 & 0 & 0 & 0 & K_{98} & K_{99} & K_{910} \\ 0 & 0 & 0 & 0 & 0 & 0 & 0 & 0 & K_{109} & K_{1010} \end{bmatrix} \begin{Bmatrix} \hat{u}_1 \\ \hat{u}_2 \\ \hat{u}_3 \\ \hat{u}_4 \\ \hat{u}_5 \\ \hat{u}_6 \\ \hat{u}_7 \\ \hat{u}_8 \\ \hat{u}_9 \\ \hat{u}_{10} \end{Bmatrix} = \begin{Bmatrix} \hat{f}_1 + \hat{K}_1^*(\hat{u}_1 - \hat{u}_6) \\ \hat{f}_2 + \hat{f}_{11} + \hat{f}_{12} \\ \hat{f}_3 + \hat{K}_2^*(\hat{u}_3 - \hat{u}_4) \\ \hat{f}_4 + \hat{K}_2^*(\hat{u}_4 - \hat{u}_3) \\ \hat{f}_5 + \hat{K}_3^*(\hat{u}_5 - \hat{u}_{10}) \\ \hat{f}_6 + \hat{K}_1^*(\hat{u}_6 - \hat{u}_1) \\ \hat{f}_7 + \hat{K}_4^*(\hat{u}_7 - \hat{u}_8) \\ \hat{f}_8 + \hat{K}_4^*(\hat{u}_8 - \hat{u}_7) \\ \hat{f}_9 + \hat{f}_{13} + \hat{f}_{14} \\ \hat{f}_{10} + \hat{K}_3^*(\hat{u}_{10} - \hat{u}_5) \end{Bmatrix} \tag{4.28}$$

Re-arranging the right hand side terms to left hand side, the global dynamic stiffness matrix becomes as,

$$\begin{bmatrix} K_{11} & K_{12} & 0 & 0 & 0 & K_{16} & 0 & 0 & 0 & 0 \\ K_{21} & K_{22} & K_{23} & 0 & 0 & 0 & 0 & 0 & K_{29} & 0 \\ 0 & K_{32} & K_{33} & K_{34} & 0 & 0 & 0 & 0 & 0 & 0 \\ 0 & 0 & K_{43} & K_{44} & K_{45} & 0 & 0 & 0 & 0 & 0 \\ 0 & 0 & 0 & K_{54} & K_{55} & 0 & 0 & 0 & 0 & K_{510} \\ K_{61} & 0 & 0 & 0 & 0 & K_{66} & K_{67} & 0 & 0 & 0 \\ 0 & 0 & 0 & 0 & 0 & K_{76} & K_{77} & K_{78} & 0 & 0 \\ 0 & 0 & 0 & 0 & 0 & 0 & K_{87} & K_{88} & K_{89} & 0 \\ 0 & K_{92} & 0 & 0 & 0 & 0 & 0 & K_{98} & K_{99} & K_{910} \\ 0 & 0 & 0 & 0 & K_{105} & 0 & 0 & 0 & K_{109} & K_{1010} \end{bmatrix} \begin{Bmatrix} \hat{u}_1 \\ \hat{u}_2 \\ \hat{u}_3 \\ \hat{u}_4 \\ \hat{u}_5 \\ \hat{u}_6 \\ \hat{u}_7 \\ \hat{u}_8 \\ \hat{u}_9 \\ \hat{u}_{10} \end{Bmatrix} = \begin{Bmatrix} F_1 \\ F_2 \\ F_3 \\ F_4 \\ F_5 \\ F_6 \\ F_7 \\ F_8 \\ F_9 \\ F_{10} \end{Bmatrix} \tag{4.29}$$

$$[\hat{k}]\ \hat{u} = \hat{F}$$

Here coefficients of the above global dynamic stiffness matrix are given by,

$$K_{11} = \hat{K}_{11}^{(1)} - \hat{K}_{1}^{*}$$
$$K_{12} = \hat{K}_{12}^{(1)}$$
$$K_{16} = \hat{K}_{1}^{*}$$
$$K_{21} = \hat{K}_{21}^{(1)}$$
$$K_{22} = \hat{K}_{22}^{(1)} + \hat{K}_{11}^{(2)} + \hat{K}_{11}^{(4)}$$
$$K_{23} = \hat{K}_{12}^{(2)}$$
$$K_{29} = \hat{K}_{12}^{(4)}$$
$$K_{32} = \hat{K}_{21}^{(2)}$$
$$K_{33} = \hat{K}_{22}^{(2)} - \hat{K}_{2}^{*}$$
$$K_{34} = \hat{K}_{2}^{*}$$
$$K_{43} = \hat{K}_{2}^{*}$$
$$K_{44} = \hat{K}_{11}^{(5)} - \hat{K}_{2}^{*}$$
$$K_{45} = \hat{K}_{12}^{(5)}$$
$$K_{54} = \hat{K}_{21}^{(5)}$$
$$K_{55} = \hat{K}_{22}^{(5)} - \hat{K}_{3}^{*}$$
$$K_{510} = \hat{K}_{3}^{*}$$
$$K_{61} = \hat{K}_{1}^{*}$$
$$K_{66} = \hat{K}_{11}^{(3)} - \hat{K}_{1}^{*}$$

$$K_{76} = \hat{K}_{21}^{(3)}$$
$$K_{77} = \hat{K}_{22}^{(3)} - \hat{K}_{4}^{*}$$
$$K_{78} = \hat{K}_{4}^{*}$$
$$K_{87} = \hat{K}_{4}^{*}$$
$$K_{88} = \hat{K}_{11}^{(6)} - \hat{K}_{4}^{*}$$
$$K_{89} = \hat{K}_{12}^{(6)}$$
$$K_{92} = \hat{K}_{21}^{(4)}$$
$$K_{98} = \hat{K}_{21}^{(6)}$$
$$K_{99} = \hat{K}_{22}^{(5)} + \hat{K}_{11}^{(7)} + \hat{K}_{22}^{(4)}$$
$$K_{910} = \hat{K}_{12}^{(7)}$$
$$K_{105} = \hat{K}_{3}^{*}$$
$$K_{109} = \hat{K}_{21}^{(7)}$$
$$K_{1010} = \hat{K}_{22}^{(7)} - \hat{K}_{3}^{*}$$

$$F_1 = \hat{f}_1$$
$$F_2 = \hat{f}_2 + \hat{f}_{11} + \hat{f}_{12}$$
$$F_3 = \hat{f}_3$$
$$F_4 = \hat{f}_4$$
$$F_5 = \hat{f}_5$$
$$F_6 = \hat{f}_6$$
$$F_7 = \hat{f}_7$$
$$F_8 = \hat{f}_8$$
$$F_9 = \hat{f}_9 + \hat{f}_{13} + \hat{f}_{14}$$
$$F_{10} = \hat{f}_{10}$$

4.5 Global dynamic stiffness matrix of 2D beam-frame model

The stiffness matrix of the beam-frame model is taken into two instants one is due to the beam elements and the other due to the distributed springs. So after adding these two matrices, the global stiffness matrix of the 2D beam-frame model of the wing is obtained.

4.6 Summary

Through this global stiffness matrix the frequency response analysis of the 2D beam-frame model has been performed. The response history at all nodal points had obtained in the frequency domain due to the high frequency loading at tip node.

Chapter 5

Results and Discussions

This chapter comprises of two major parts first half includes response analysis for 1D rod, 1D beam and 2D frame using spectral finite element method. The second half includes two different cases of 2D beam-frame model of aircraft wing using the formulation from the previous chapter of this dissertation.

5.1 Dynamic Response of an Isotropic Rod

Consider a semi-infinite rod, fixed at one end and impacted at the other end. Model has two elements, first element is of finite length and second element is considered as extending to infinity (a throw-off element). A throw-off element is introduced in order to avoid reflections from the boundary.

The 1D rod of aluminum has been taken with material properties as follows,

Elastic modulus: 70 GPa
Shear modulus: 26.9 GPa
Cross-section: $10 \times 10mm^2$
Length of the rod: 1m

The axial load is applied at node 3 and axial velocity history is measured at the same.

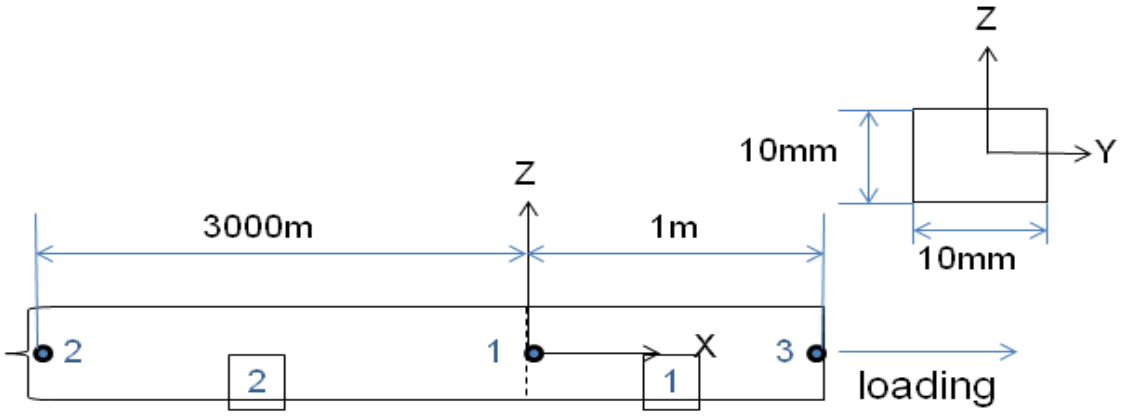

Figure 5-1 Semi-Infinite Rod Modeled with two Elements.

The following plots shows the axial velocity $\dot{u}$ history at node 3 due to high-frequency pulse in the axial direction at the same, the applied load history is shown in the inset image of each plot.

The spectrum relation of an isotropic rod for an undamped case is

$$k_1 = \omega\sqrt{\frac{\rho A}{EA}} \tag{5.1}$$

Here k_1 is linear in frequency.

For the dispersion relation, constant phase and group speeds of

$$c = \frac{\omega}{k} = \sqrt{\frac{EA}{\rho A}} = c_0, \qquad c_g = \frac{d\omega}{dk} = \sqrt{\frac{EA}{\rho A}} = c_0 \tag{5.2}$$

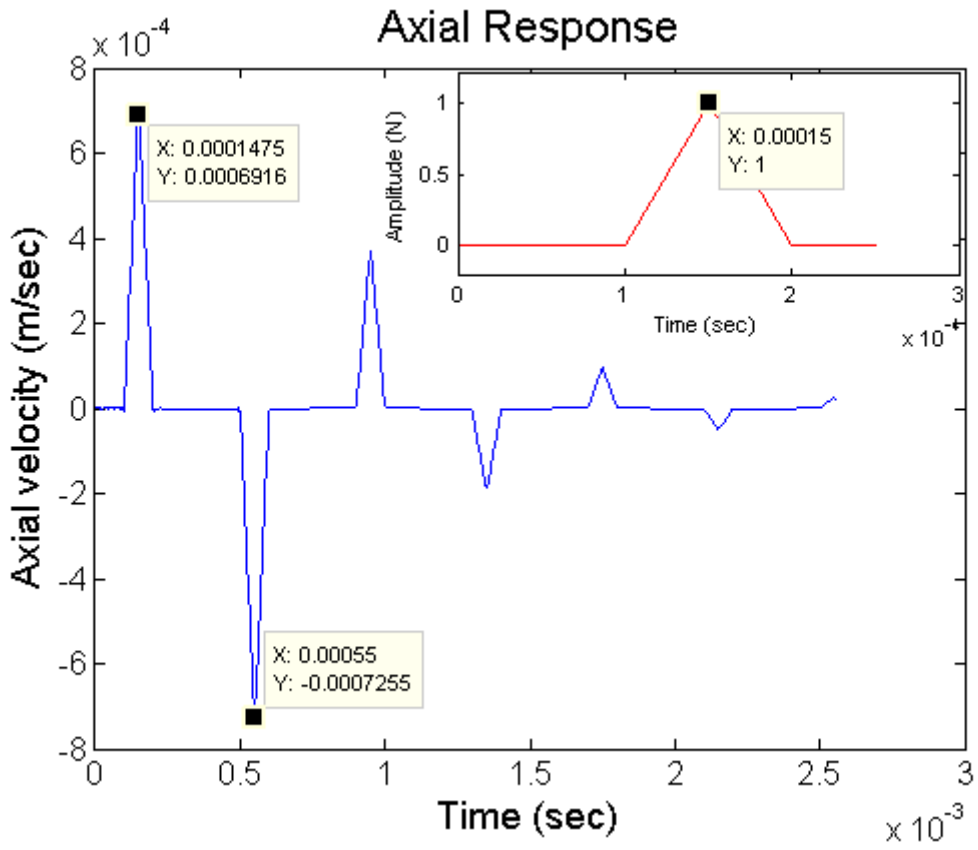

Figure 5-2 Axial Velocity history at Node-3, due to loading (inset of the plot) in the Axial direction.

Using the material properties,

From equation (5.2),

Constant speed of the wave travelling through rod = 5×10^3 m/s

Time taken by the wave to reach the interface from the free end = 0.2×10^{-3} sec

Time taken by the wave to reach back to the free end after reflecting from the interface = Time of flight = $2 \times (0.2\times10^{-3}) = 0.4\times10^{-3}$ sec

From the above plot,

Time of launch of the pulse = 0.1475×10^{-3} sec

Time of reflection of the pulse = 0.55×10^{-3} sec

Time of flight of the pulse = 0.4025×10^{-3} sec

The time of flight of the pulse in the response history is equal to that predicted using material properties.

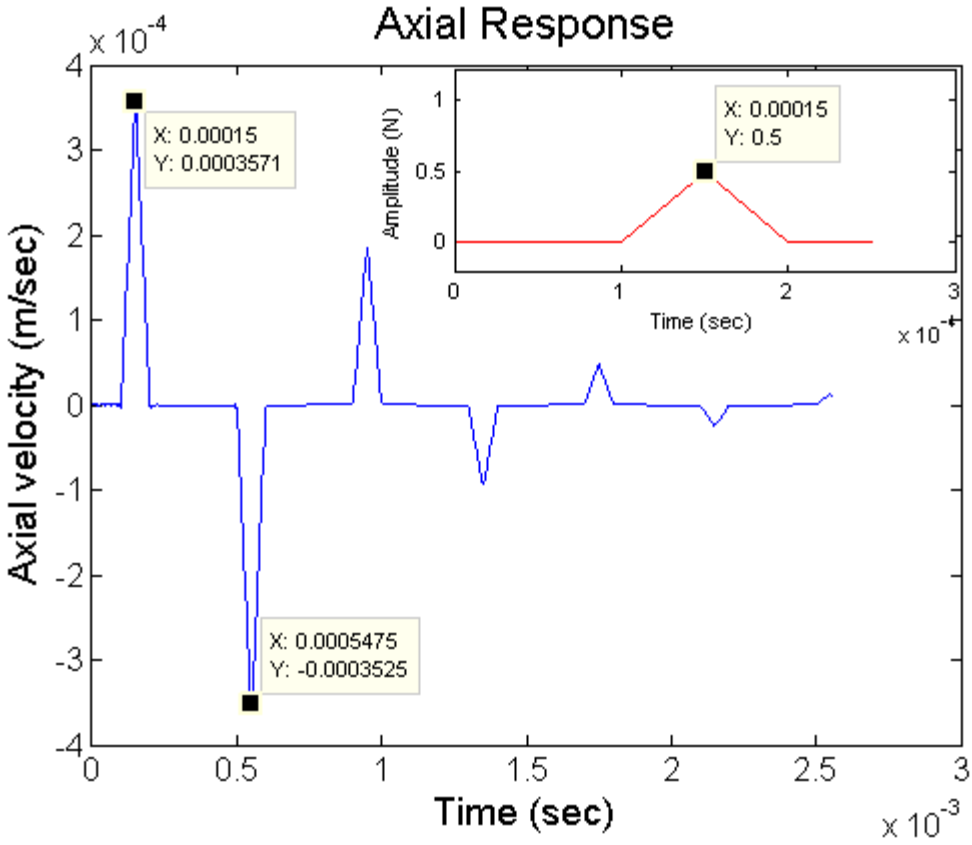

Figure 5-3 Axial Velocity history at Node-3, due to loading (inset of the plot) in the Axial direction.

Using the material properties,

From equation (5.2),

Constant speed of the wave travelling through rod = 5×10^{3} m/s

Time taken by the wave to reach the interface from the free end = 0.2×10^{-3} sec

Time taken by the wave to reach back to the free end after reflecting from the interface = Time of flight = $2 \times (0.2 \times 10^{-3}) = 0.4 \times 10^{-3}$ sec

From the above plot,

Time of launch of the pulse = 0.15×10^{-3} sec

Time of reflection of the pulse = 0.5475×10^{-3} sec

Time of flight of the pulse = 0.3975×10^{-3} sec

The time of flight of the pulse in the response history is equal to that predicted using material properties.

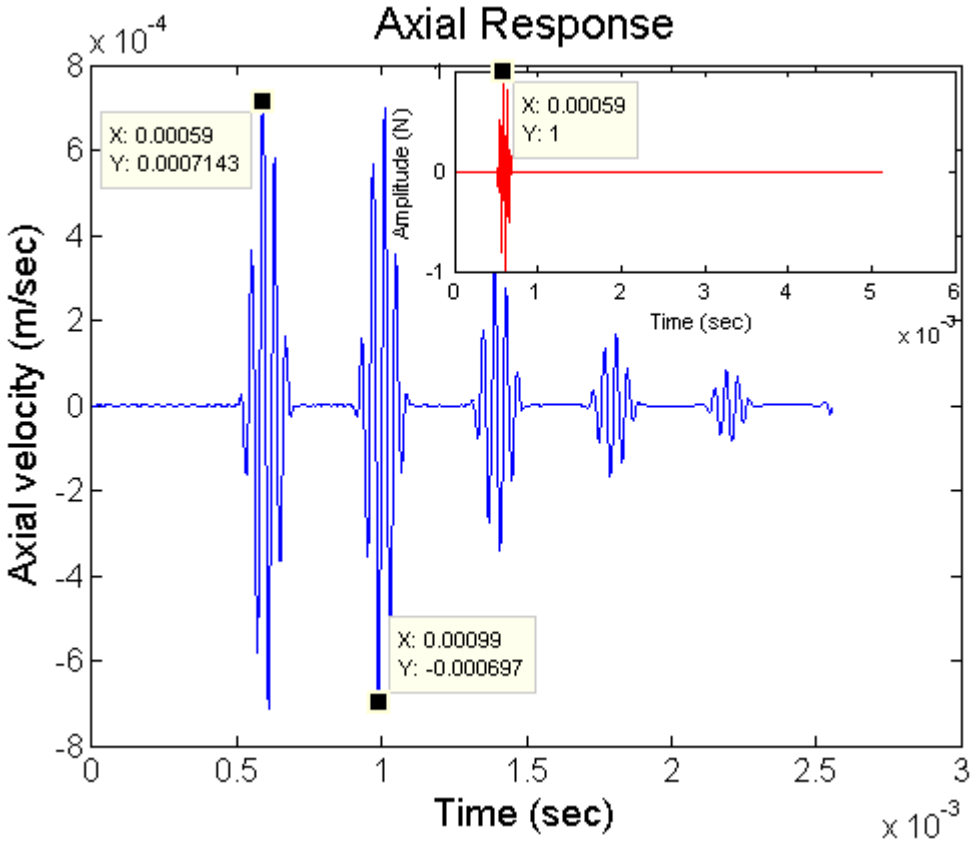

Figure 5-4 Axial Velocity history at Node-3, due to loading (inset of the plot) in the Axial direction.

Using the material properties,

From equation (5.2),

Constant speed of the wave travelling through rod = 5×10^{3} m/s

Time taken by the wave to reach the interface from the free end = 0.2×10^{-3} sec

Time taken by the wave to reach back to the free end after reflecting from the interface = Time of flight = $2 \times (0.2 \times 10^{-3}) = 0.4 \times 10^{-3}$ sec

From the above plot,

Time of launch of the pulse = 0.59×10^{-3} sec

Time of reflection of the pulse = 0.99×10^{-3} sec

Time of flight of the pulse = 0.4×10^{-3} sec

The time of flight of the pulse in the response history is equal to that predicted using material properties.

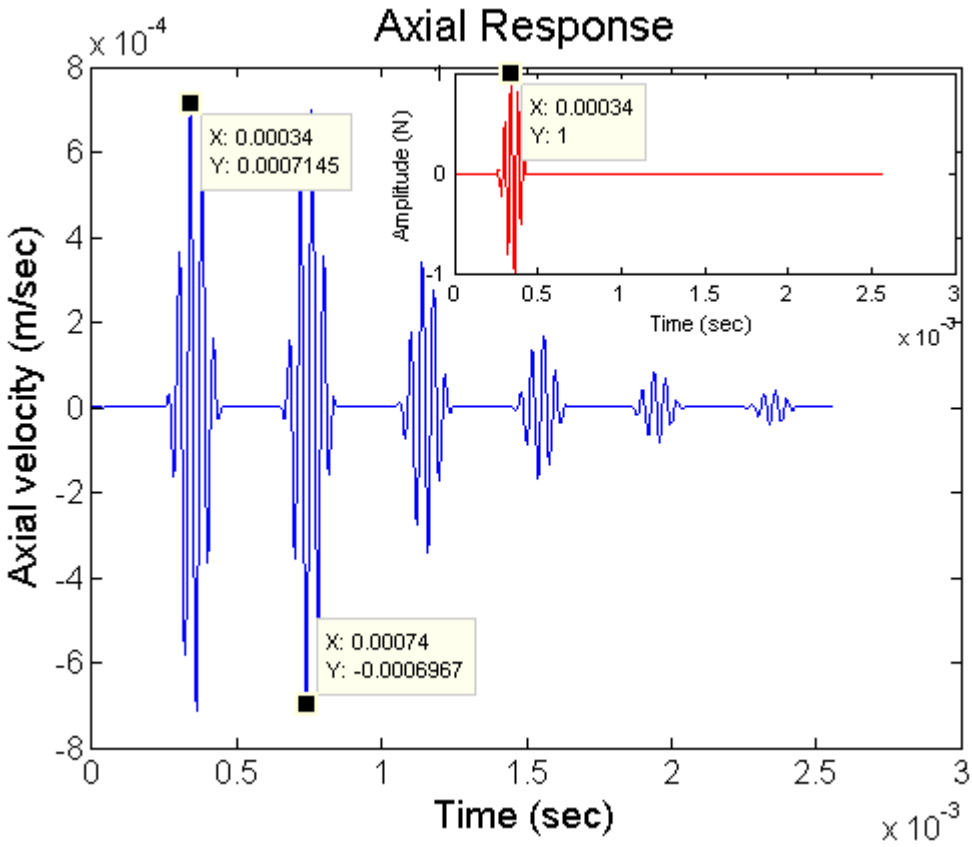

Figure 5-5 Axial Velocity history at Node-3, due to loading (inset of the plot) in the Axial direction.

Using the material properties,

From equation (5.2),

Constant speed of the wave travelling through rod = 5×10^{3} m/s

Time taken by the wave to reach the interface from the free end = 0.2×10^{-3} sec

Time taken by the wave to reach back to the free end after reflecting from the interface = Time of flight = $2 \times (0.2\times10^{-3}) = 0.4\times10^{-3}$ sec

From the above plot,

Time of launch of the pulse = 0.34×10^{-3} sec

Time of reflection of the pulse = 0.74×10^{-3} sec

Time of flight of the pulse = 0.4×10^{-3} sec

The time of flight of the pulse in the response history is equal to that predicted using material properties.

5.2 Dynamic Response of an Isotropic Beam

Consider a semi-infinite Euler-Bernoulli beam, fixed at one end and impacted at the other end. Model has two elements, first element is of finite length and second element is a throw-off element. A throw-off element is introduced in order to avoid reflections from the boundary.

The 1D beam of aluminum has been taken with material properties as follows,

Elastic modulus: 70 GPa
Shear modulus: 26.9 GPa
Cross-section: $10 \times 10mm^2$
Length of the beam: 1m

The transverse load is applied at the node 3 and transverse velocity history is measured at the same.

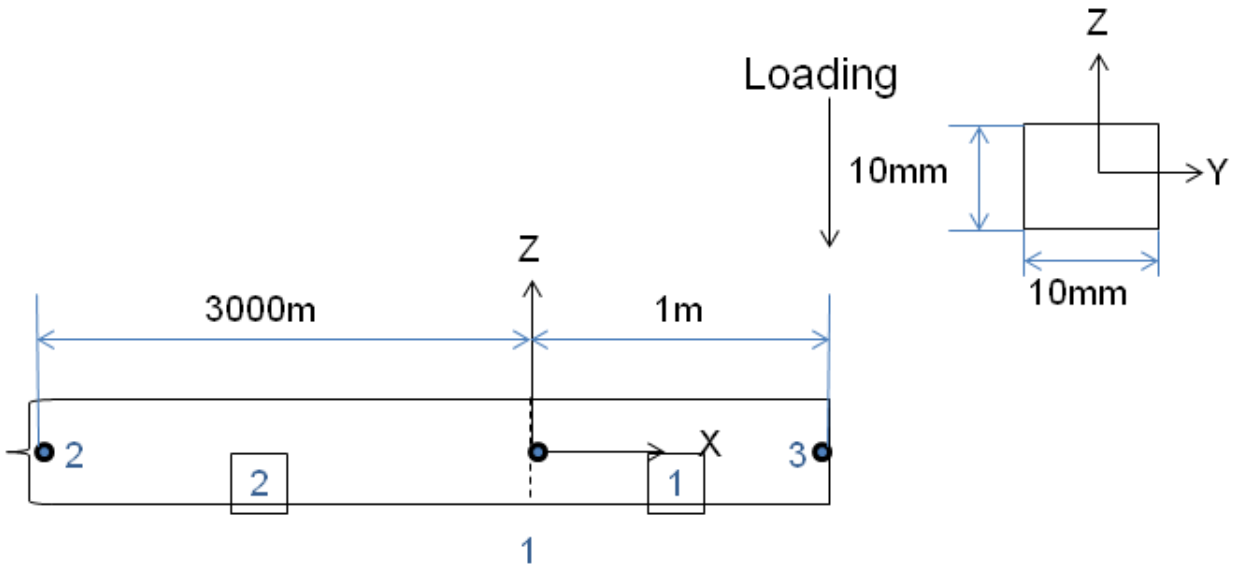

Figure 5-6 Semi-Infinite Beam Modeled with Two Elements.

The following plots shows the transverse velocity $\dot{w}$ history at node 3 due to high-frequency pulse in the transverse direction at the same, the applied load history is shown in the inset image of each plot.

The spectrum relation of an isotropic beam for an undamped case is

$$k_1 = \pm\sqrt[4]{\frac{\omega^2 \rho A}{EI}}, \qquad k_2 = \pm i\sqrt[4]{\frac{\omega^2 \rho A}{EI}} \tag{5.3}$$

The mode 2 behavior is entirely imaginary for the undamped case, hence there is no propagation behavior for this mode. Considering only the mode 1 wave motion gives the phase speed and group speed as

$$c = \frac{\omega}{k} = \sqrt{\omega}\left[\frac{EI}{\rho A}\right]^{\frac{1}{4}}, \qquad c_g = \frac{d\omega}{dk} = 2\sqrt{\omega}\left[\frac{EI}{\rho A}\right]^{\frac{1}{4}} = 2c \tag{5.4}$$

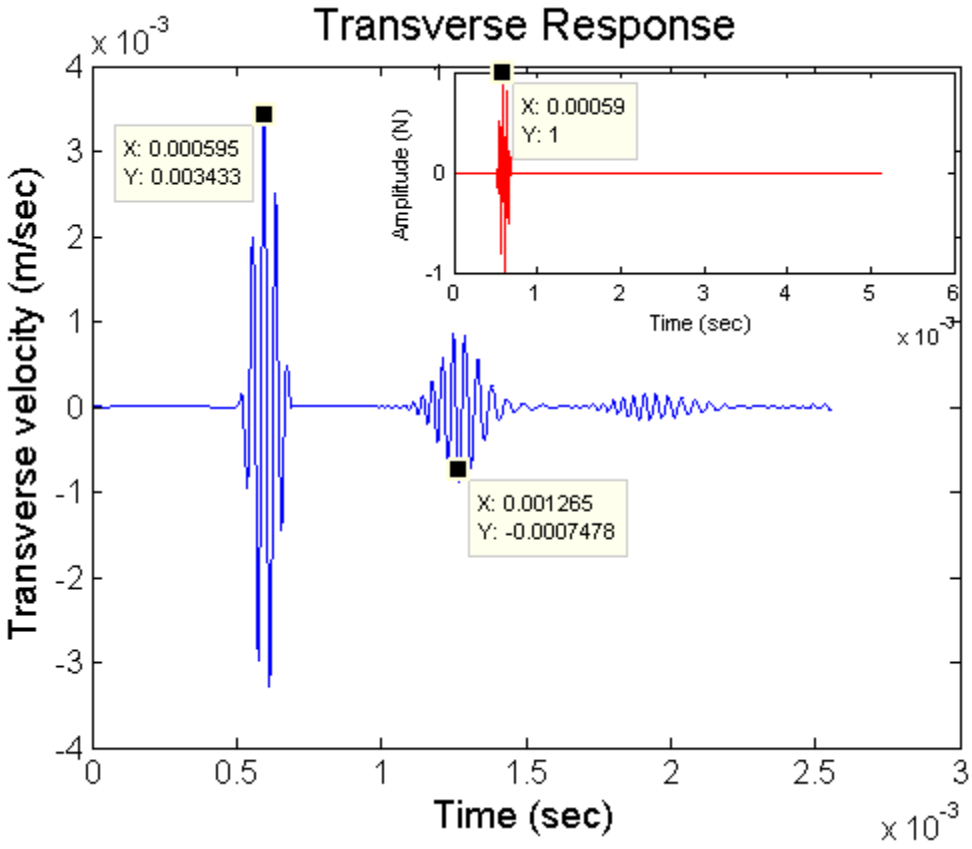

Figure 5-7 Transverse velocity history at node 3 due to loading in the inset of the plot.

Using the material properties,

From equation (5.4),

Group speed of the wave travelling through beam = 3.011×10^{3} m/s

Time taken by the wave to reach the interface from the free end = 0.332×10^{-3} sec

Time taken by the wave to reach back to the free end after reflecting from the interface = Time of flight = $2 \times (0.332\times10^{-3}) = 0.664\times10^{-3}$ sec

From the above plot,

Time of launch of the pulse = 0.595×10^{-3} sec

Time of reflection of the pulse = 1.265×10^{-3} sec

Time of flight of the pulse = 0.67×10^{-3} sec

The time of flight of the pulse in the response history is equal to that predicted using material properties.

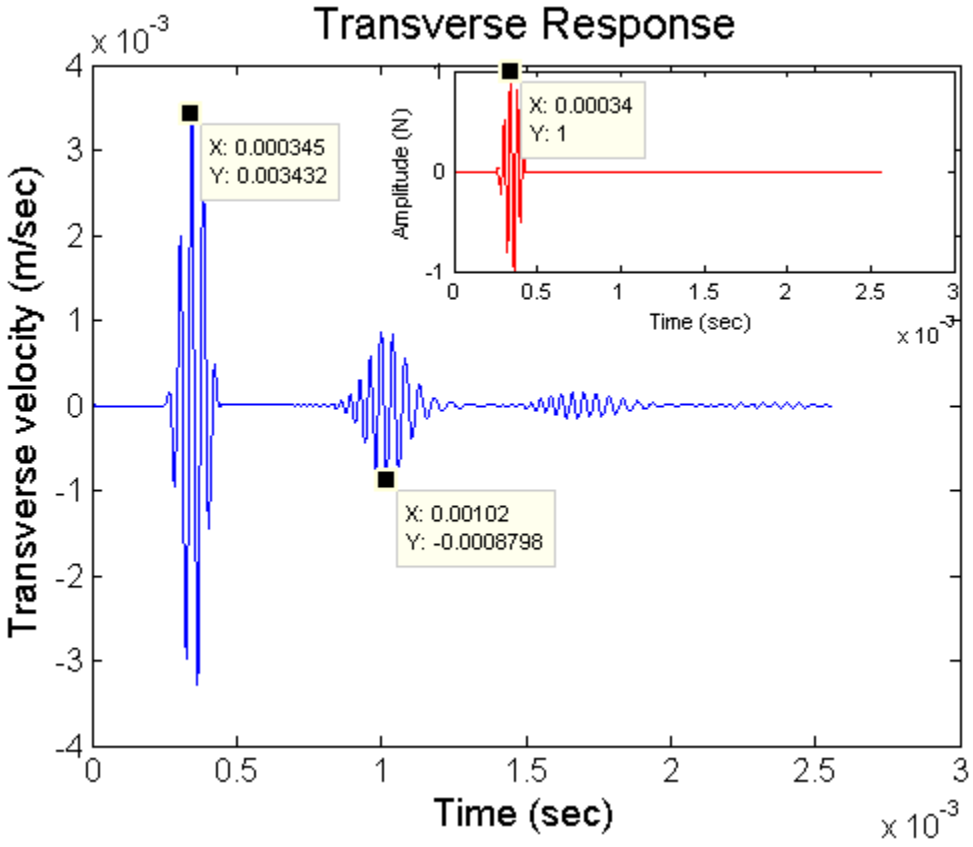

Figure 5-8 Transverse velocity history at node 3 due to loading in the inset of the plot.

Using the material properties,

From equation (5.4),

Group speed of the wave travelling through beam = 3.011×10^{3} m/s

Time taken by the wave to reach the interface from the free end = 0.332×10^{-3} sec

Time taken by the wave to reach back to the free end after reflecting from the interface = Time of flight = $2 \times (0.332\times10^{-3}) = 0.664\times10^{-3}$ sec

From the above plot,

Time of launch of the pulse = 0.345×10^{-3} sec

Time of reflection of the pulse = 1.02×10^{-3} sec

Time of flight of the pulse = 0.67×10^{-3} sec

The time of flight of the pulse in the response history is equal to that predicted using material properties.

5.3 Dynamic Response of an 2D Frame

Consider a 2D frame which is taken as a combination of 1D beam elements, for finite structures such as frame shown in figure () the propagating pulse has many reflections

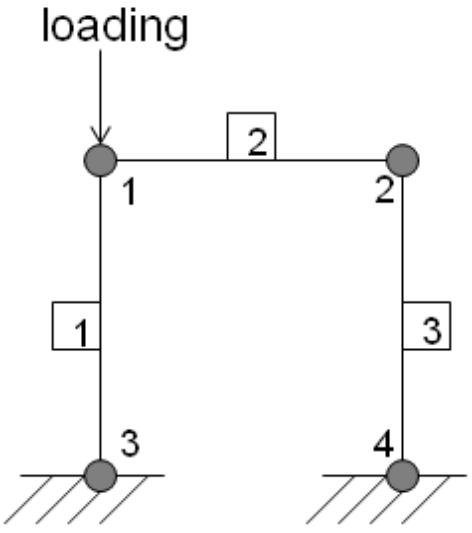

Figure 5-9 2D Frame.

A characteristic of connected structure is that they introduce sharp spectral peaks in the responses.

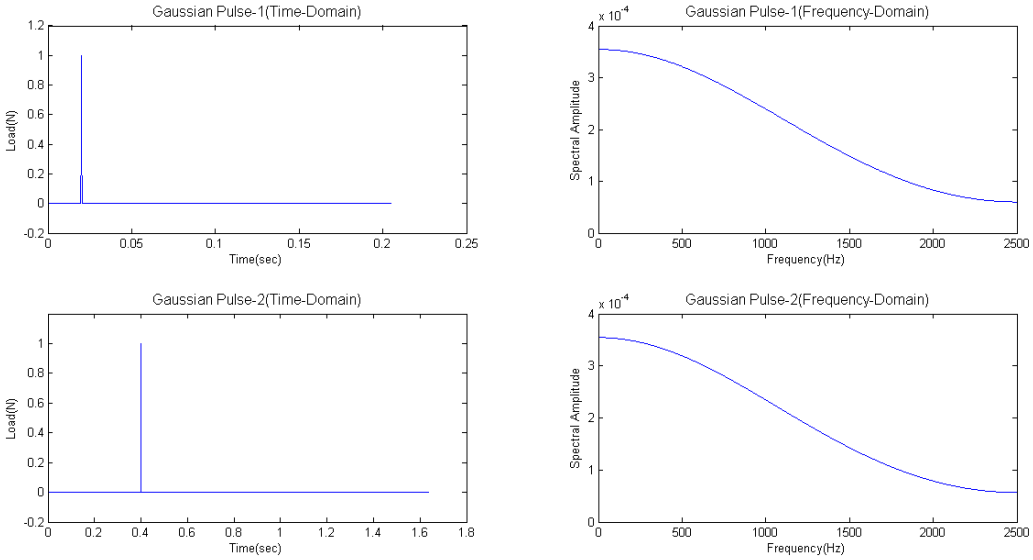

Figure 5-10 Gaussian Pulse Loading-1 and Gaussian Pulse Loading-2.

The following plots show the transverse velocity v/s Frequency at the node 1 , node 2 respectively, due to high-frequency pulse in the transverse direction at the node 1, respective load case is mentioned. The load histories are plotted in figure 5.10.

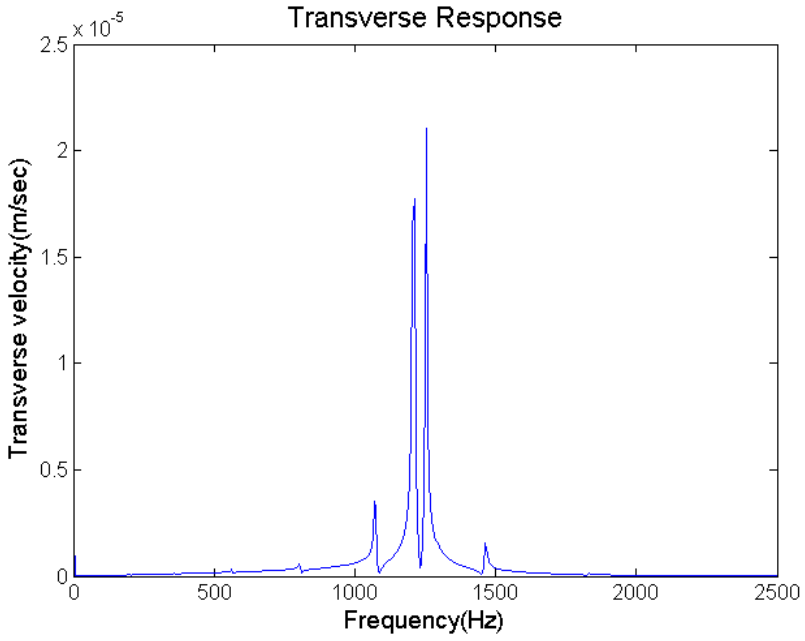

Figure 5-11 Transverse frequency response at node 1 due to Gaussian pulse_1.

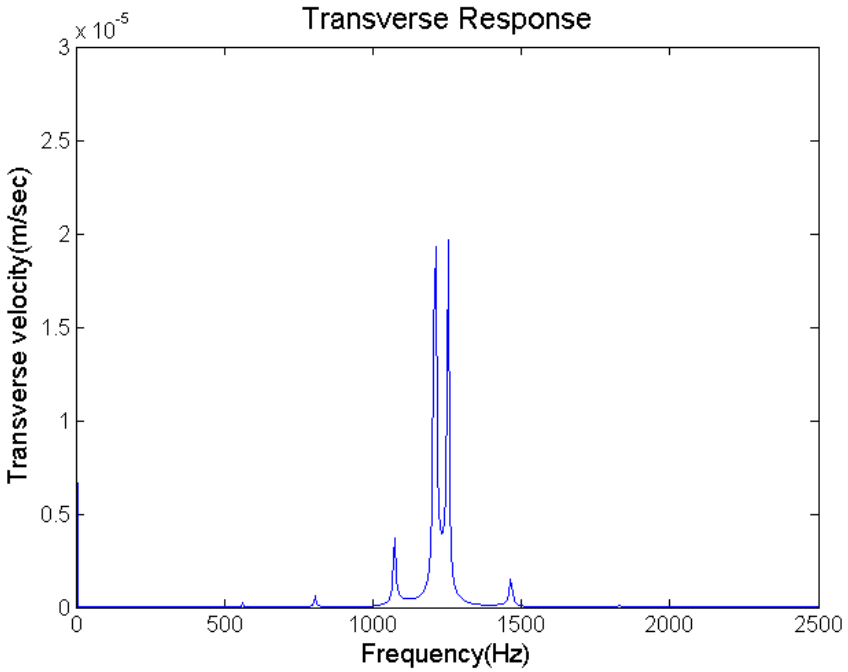

Figure 5-12 Transverse frequency response at node 2 due to Gaussian pulse_1.

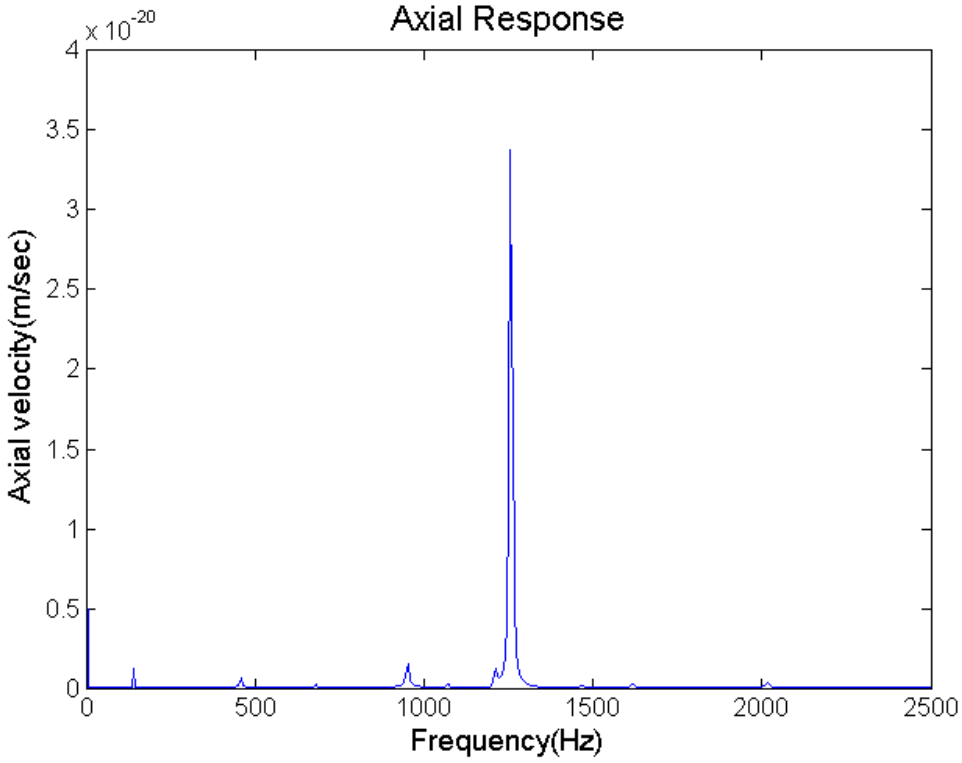

Figure 5-13 Axial frequency response at node 1 due to Gaussian pulse_1.

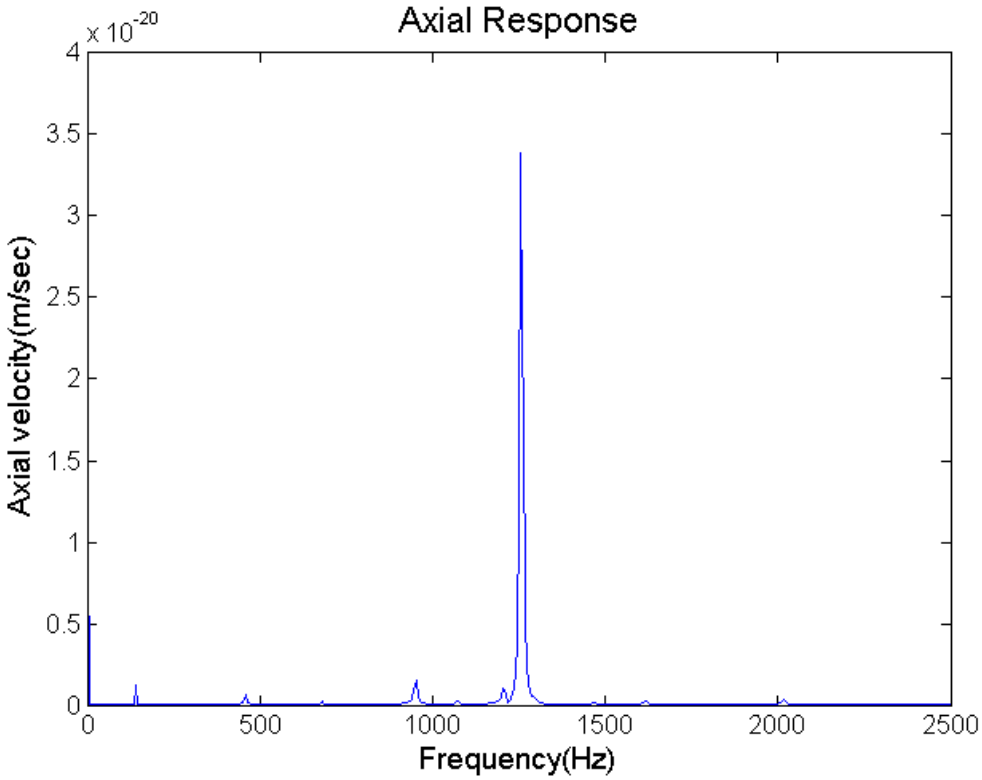

Figure 5-14 Axial frequency response at node 2 due to Gaussian pulse_1.

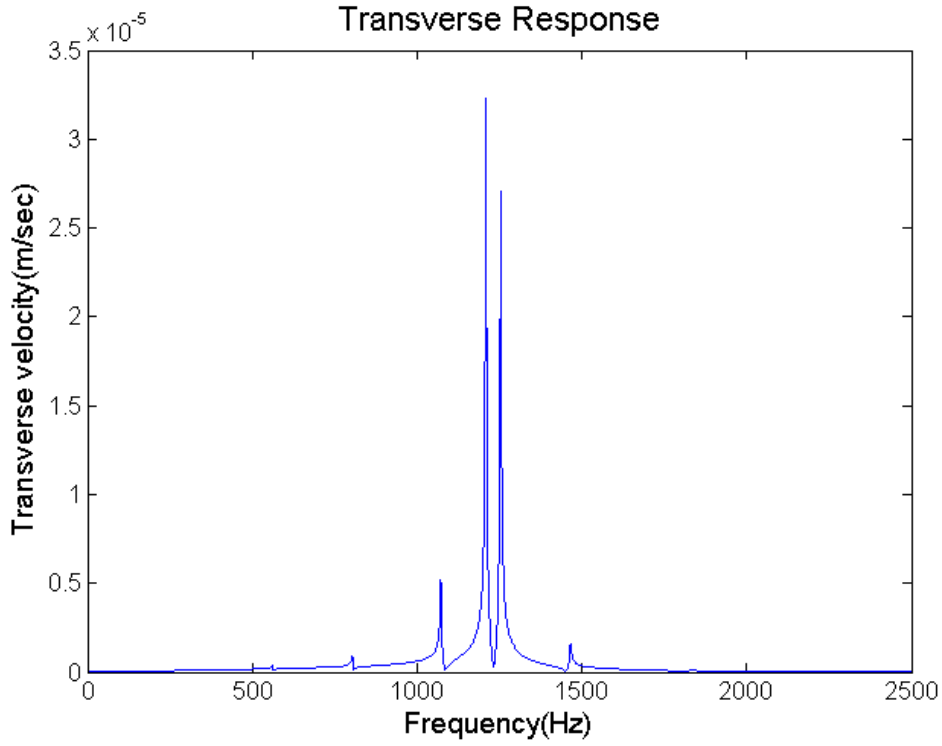

Figure 5-15 Transverse frequency response at node 1 due to Gaussian pulse_2.

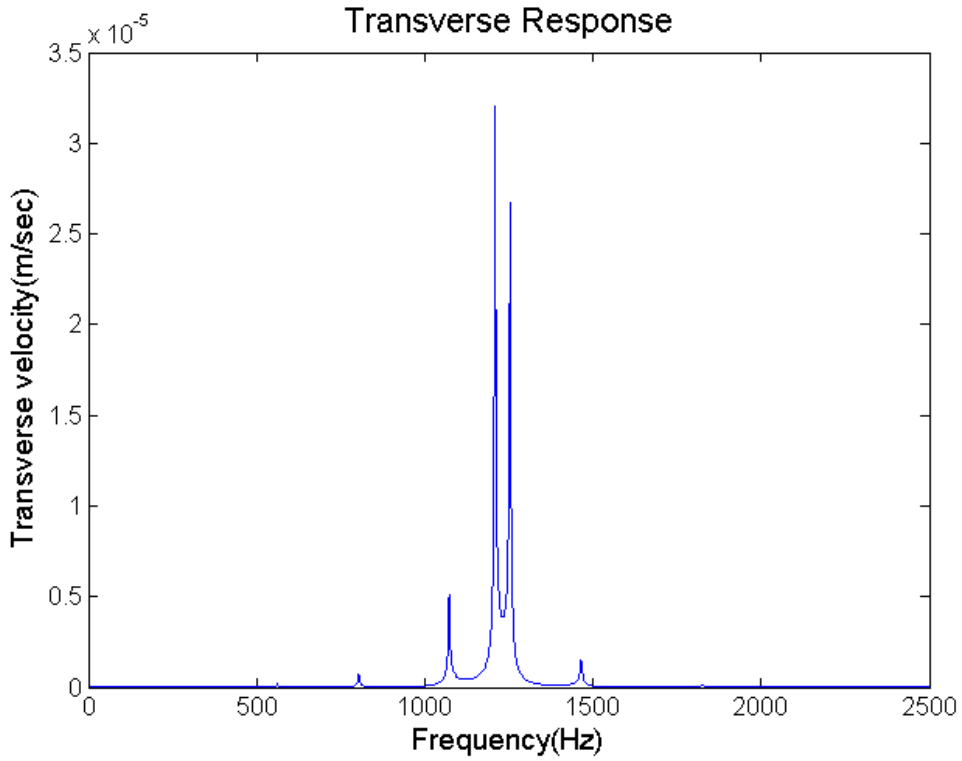

Figure 5-16 Transverse frequency response at node 2 due to Gaussian pulse_2.

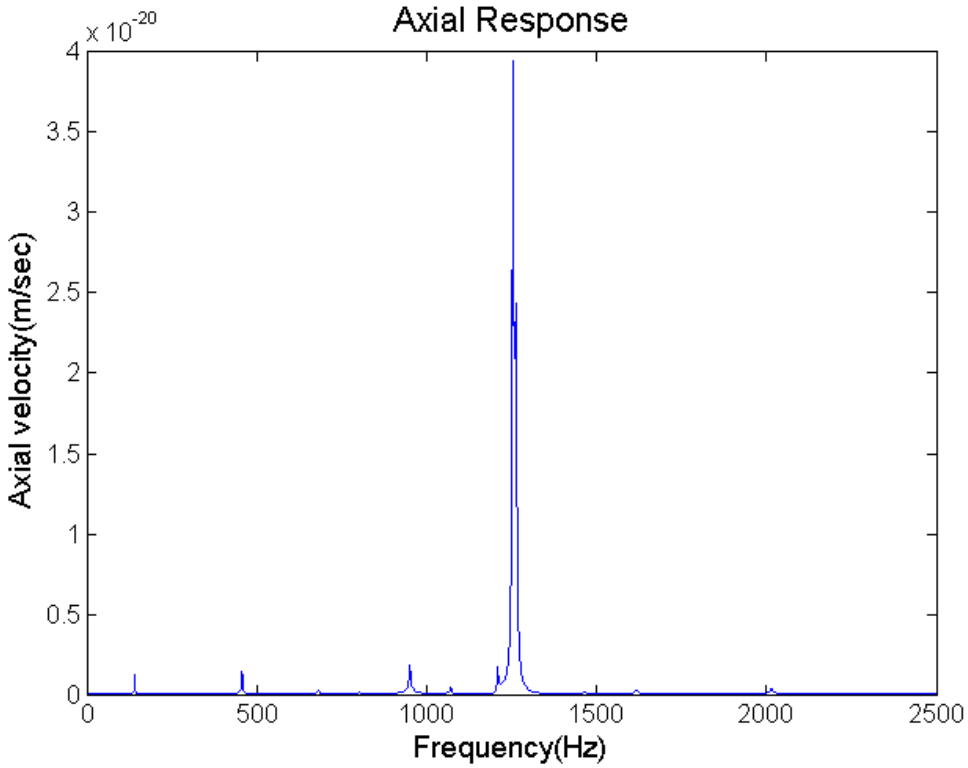

Figure 5-17 Axial frequency response at node 1 due to Gaussian pulse_2.

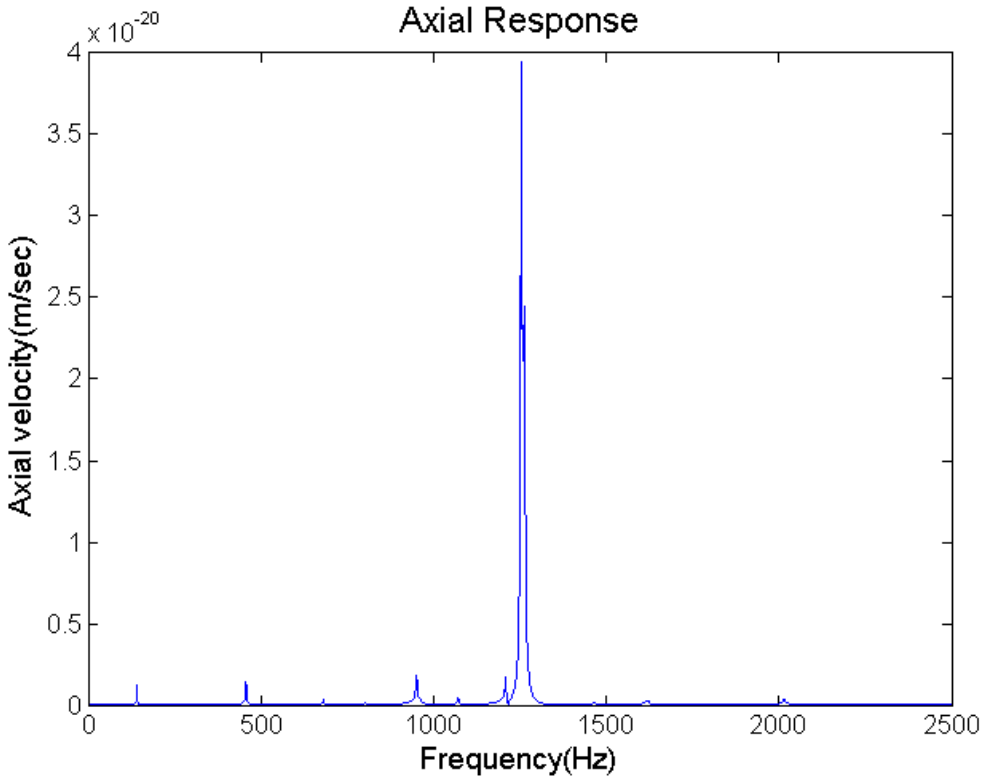

Figure 5-18 Axial frequency response at node 2 due to Gaussian pulse_2.

5.4 Frequency Response analysis of an 2D beam-frame model of aircraft wing

The 2D Beam-Frame model is replaced with 3D model of the aircraft wing for performing frequency response analysis using spectral finite element method. There are two cases which are solved as benchmark problems each separately using the formulation done in the previous chapter of this dissertation.

5.4.1 Case1: Straight wing

Here a CATIA model is prepared with two spars, six ribs and skin covering from top and bottom, the wing span is 1m and constant chord length of 0.85m and constant thickness of the airfoil as 0.082m.

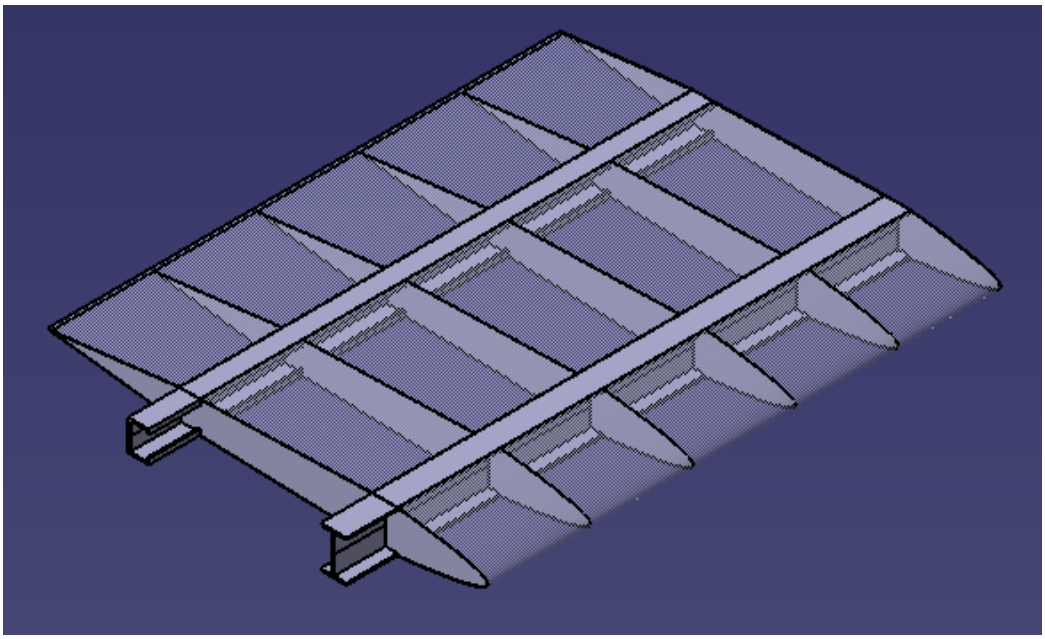

Figure 5-19 Isometric View of CATIA model of Straight Wing.

This 3D model can be replaced with the following beam-frame model to perform frequency response analysis using spectral finite element method.

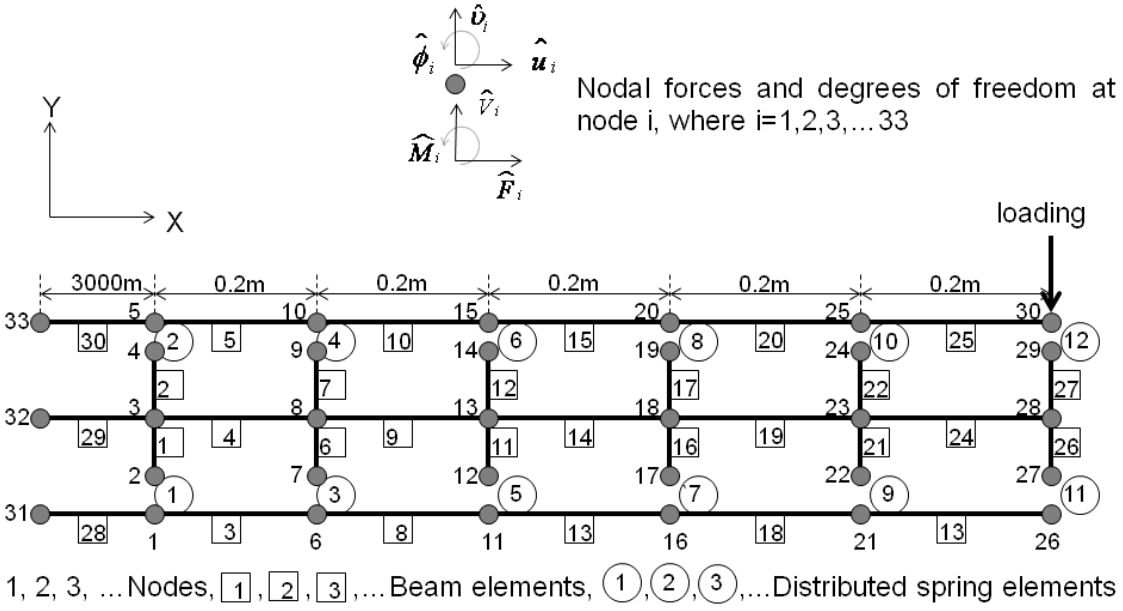

Figure 5-20 Beam-Frame Model of Straight Wing.

The following plots shows the axial velocity v/s Frequency, transverse velocity v/s Frequency at node 30, 20 due to high-frequency pulse in the transverse direction at node 30, the load time history, frequency spectrum is shown in the inset image of each plot.

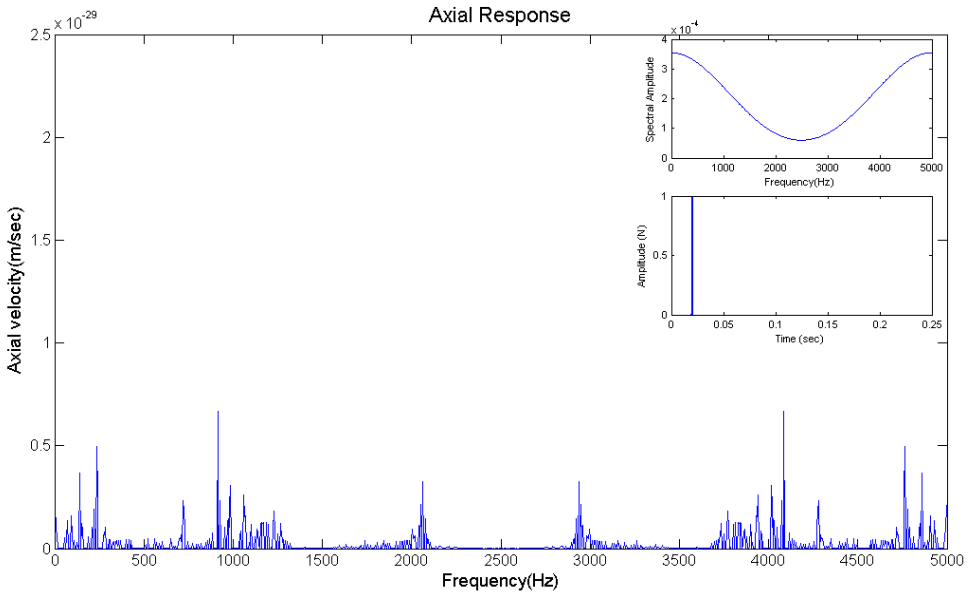

Figure 5-21 Axial velocity v/s Frequency at node 30 due to the loading (inset of the plot) in the Transverse direction.

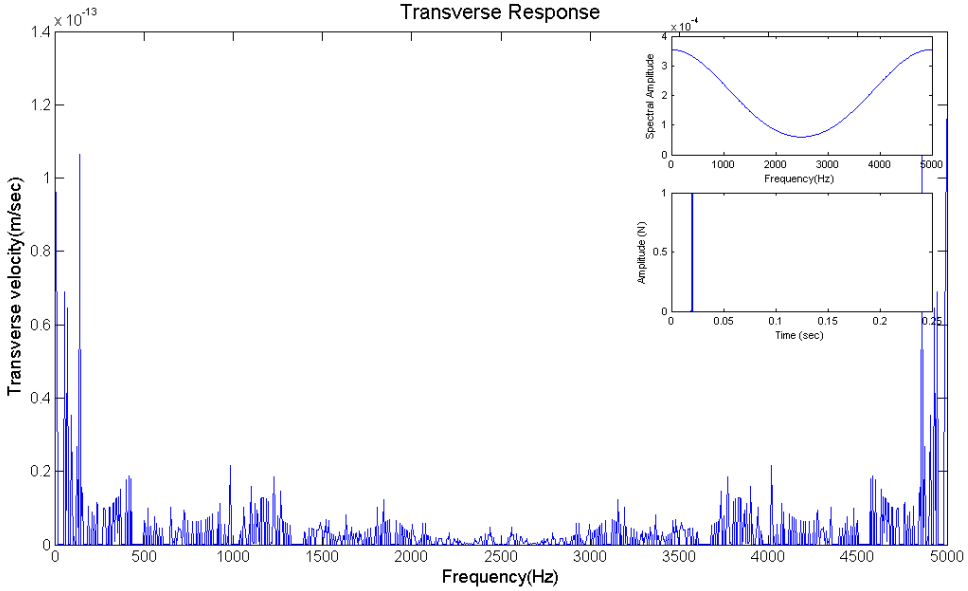

Figure 5-22 Transverse velocity v/s Frequency at node 30 due to the loading (inset of the plot) in the Transverse direction.

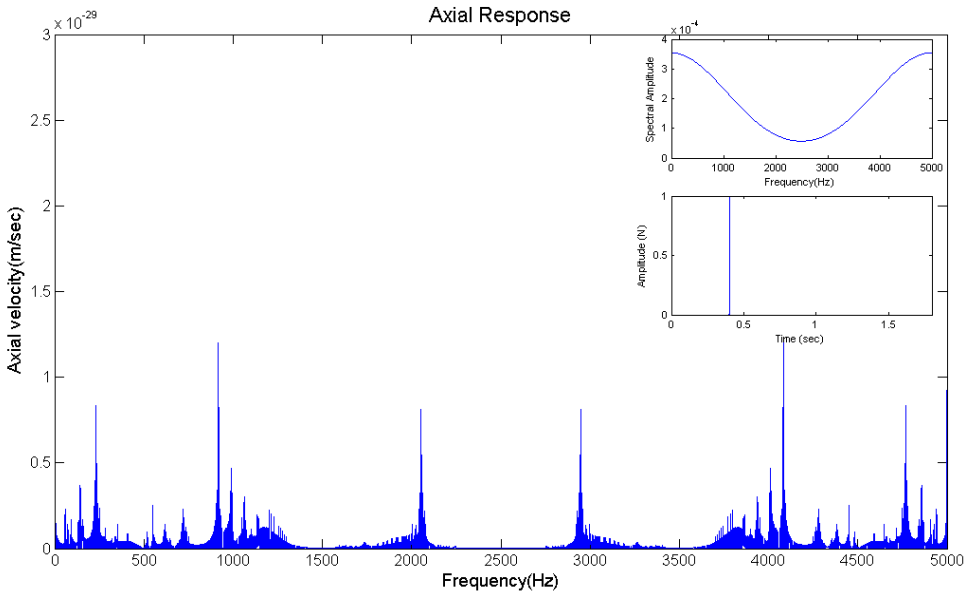

Figure 5-23 Axial velocity v/s Frequency at node 30 due to the loading (inset of the plot) in the Transverse direction.

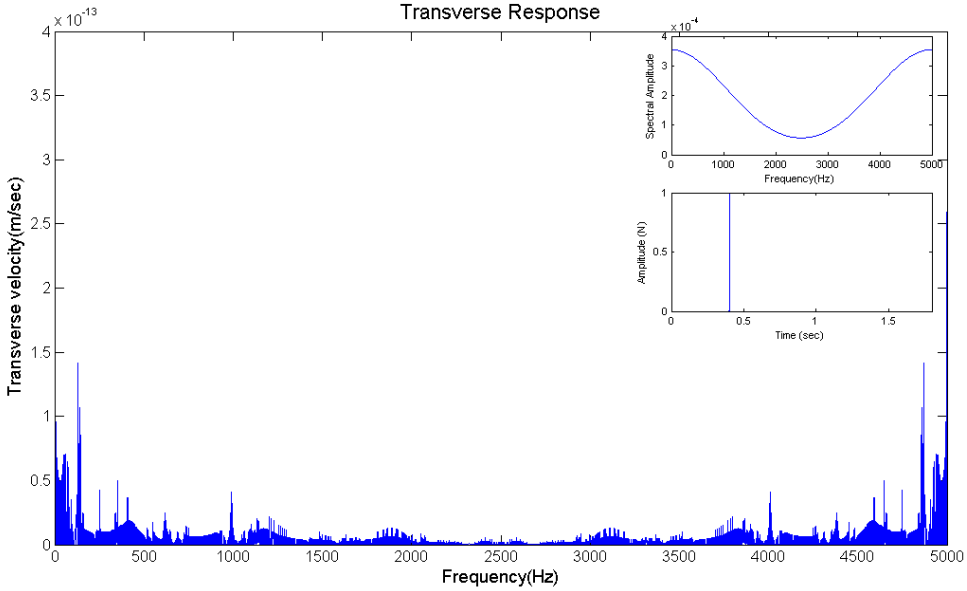

Figure 5-24 Transverse velocity v/s Frequency at node 30 due to the loading (inset of the plot) in the Transverse direction.

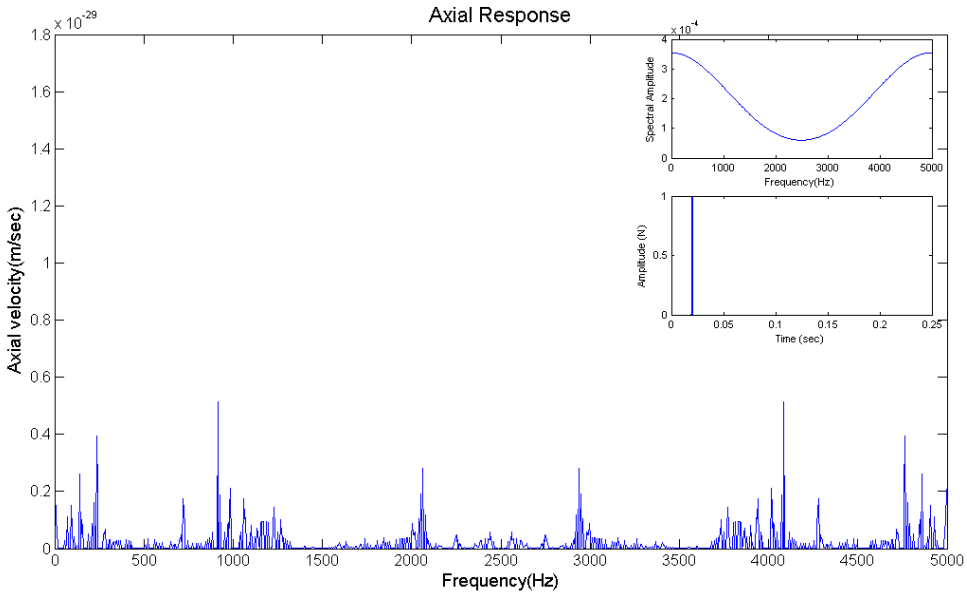

Figure 5-25 Axial velocity v/s Frequency at node 20 due to the loading (inset of the plot) in the Transverse direction.

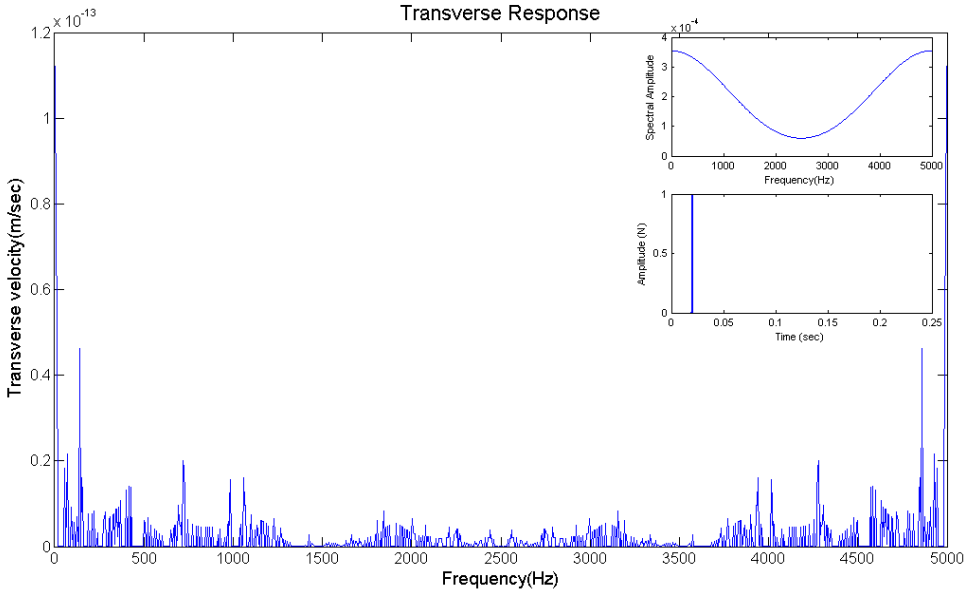

Figure 5-26 Transverse velocity v/s Frequency at node 20 due to the loading (inset of the plot) in the Transverse direction.

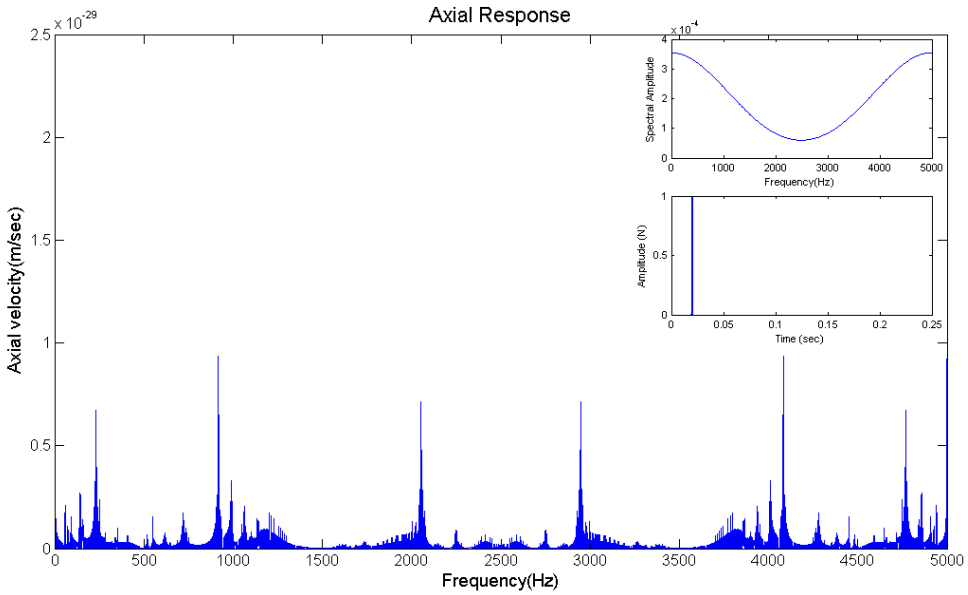

Figure 5-27 Axial velocity v/s Frequency at node 20 due to the loading (inset of the plot) in the Transverse direction.

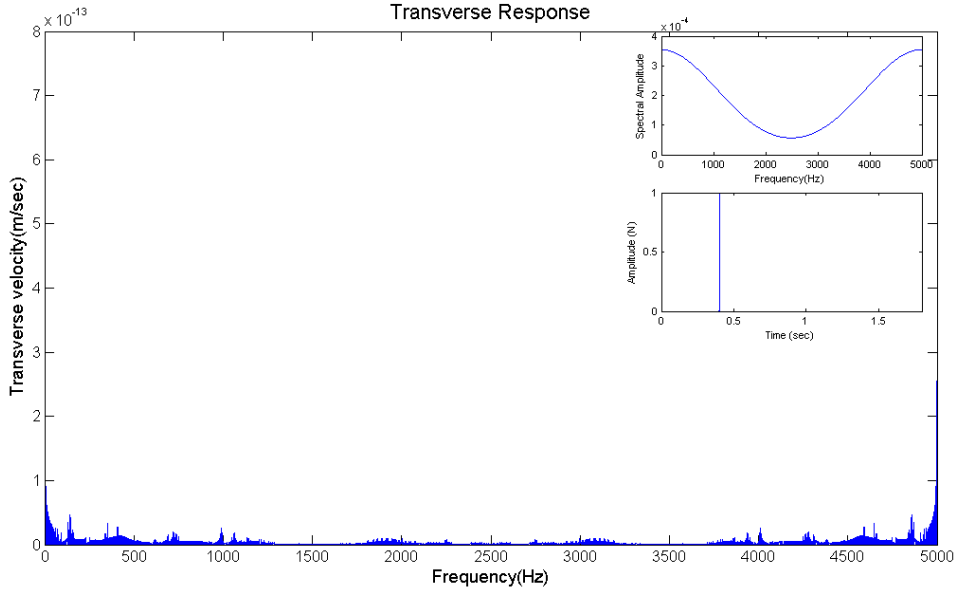

Figure 5-28 Transverse velocity v/s Frequency at node 20 due to the loading (inset of the plot) in the Transverse direction.

The following plots show a comparison of four cases Here first is healthy case, other three cases degradation of the stiffness matrix of the distributed spring is considered with steps of 0.96, 0.92 and 0.88 at spring no.10 respectively.

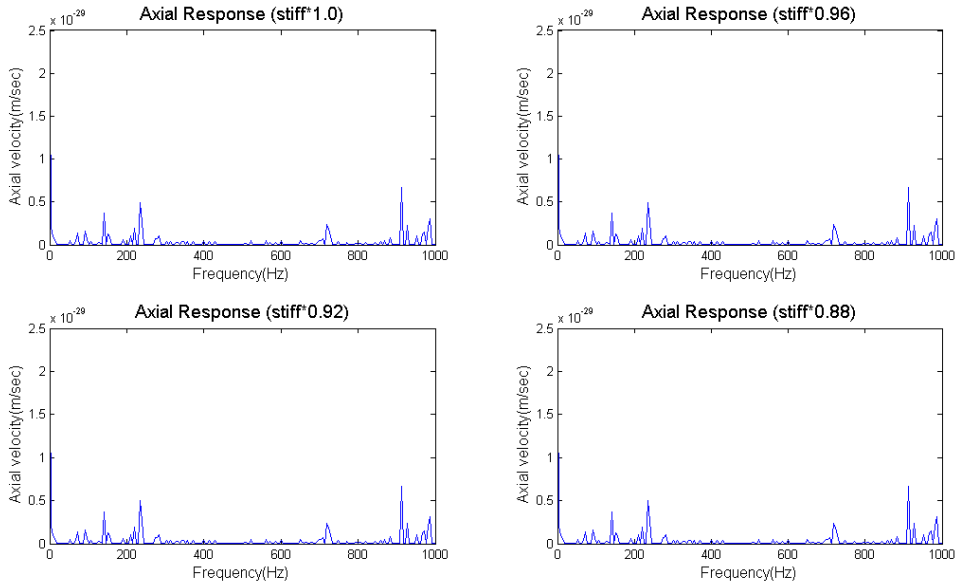

Figure 5-29 Axial velocity v/s Frequency at node 30 due to the Gaussian pulse-1.

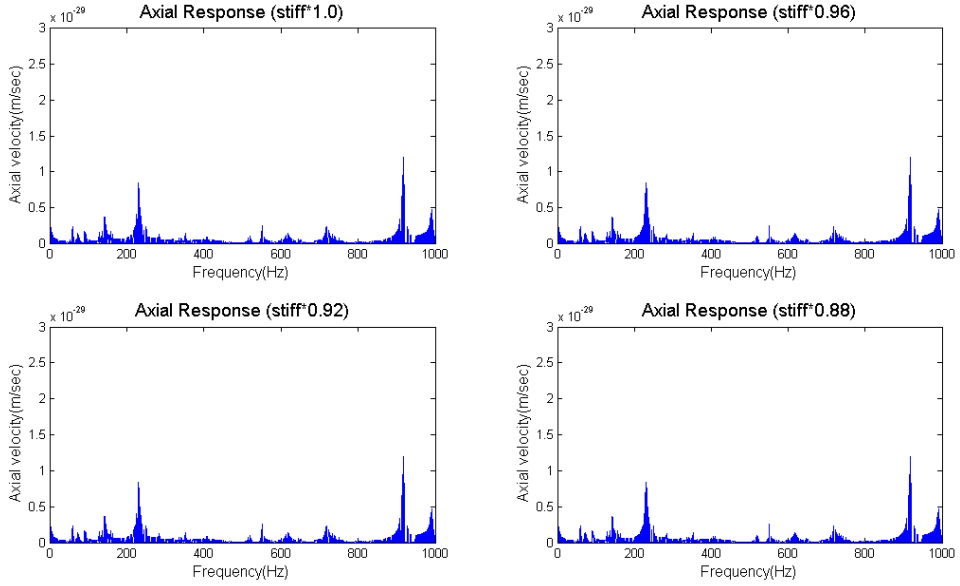

Figure 5-30 Axial velocity v/s Frequency at node 30 due to the Gaussian pulse-2.

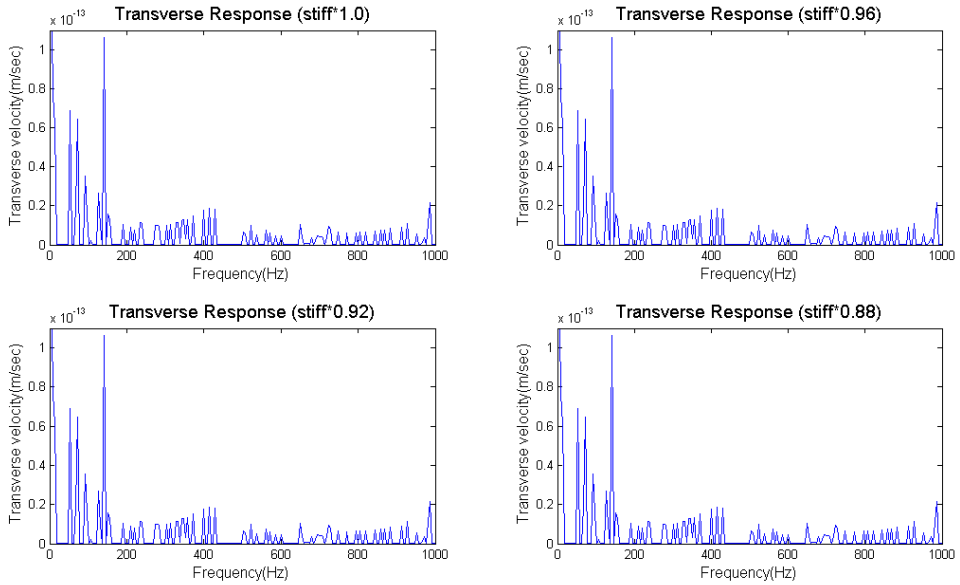

Figure 5-31 Transverse velocity v/s Frequency at node 30 due to the Gaussian pulse-1.

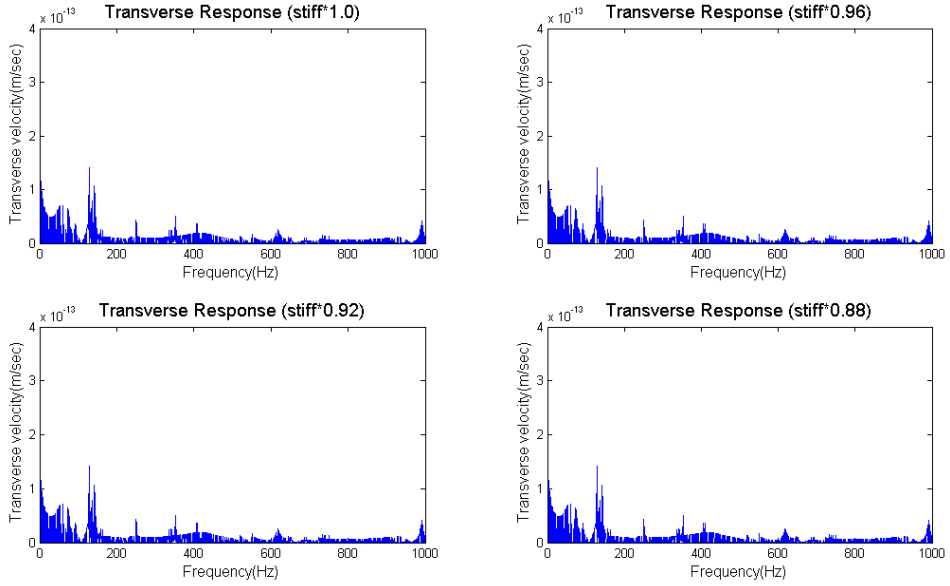

Figure 5-32 Transverse velocity v/s Frequency at node 30 due to the Gaussian pulse-2.

5.4.2 Case2: Tapered wing

This case is similar to case 2 except that the wing is tapered. Here a CATIA model is prepared with two spars, six ribs and skin covering from top and bottom, the wing span is taken as 1m and chord length varying from 0.85m at root and 0.45m at tip and constant thickness of the airfoil of the wing as 0.082m.

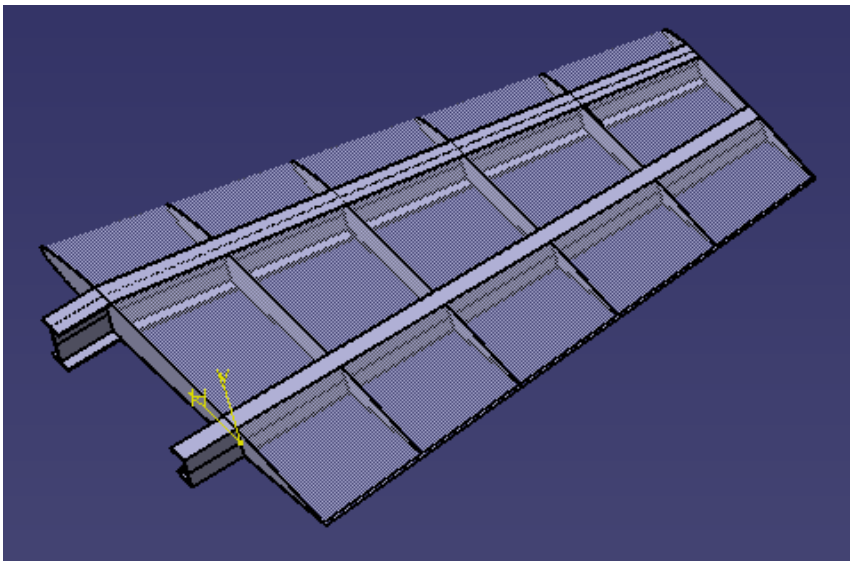

Figure 5-33 Isometric view of CATIA model of tapered wing.

This 3D model can be replaced with the following beam-frame model to perform frequency response analysis using spectral finite element method.

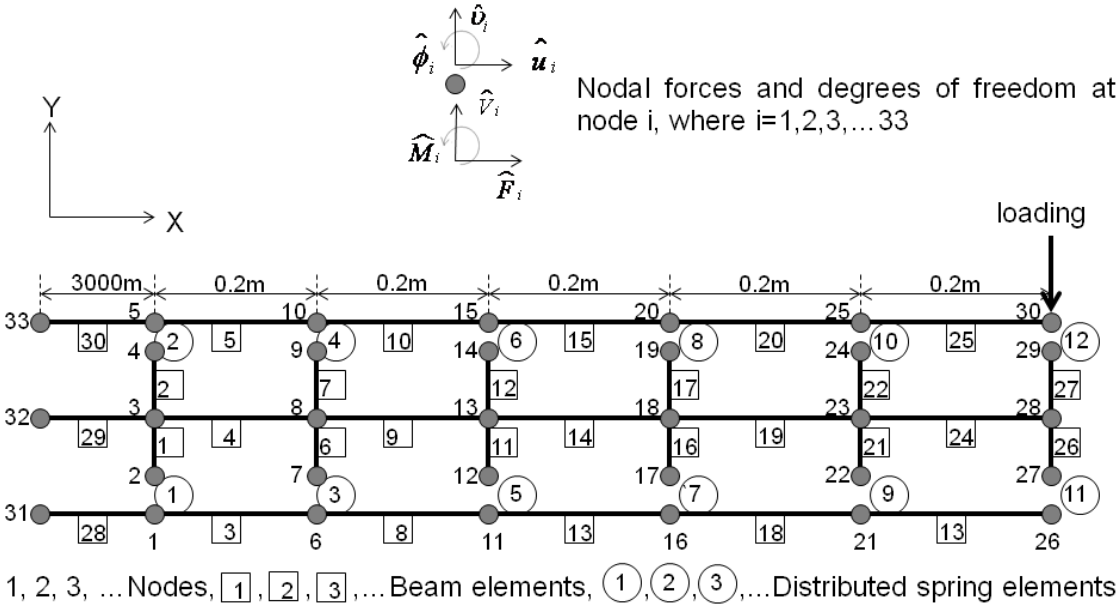

Figure 5-34 Beam-frame model of tapered wing.

The following plots shows the axial velocity v/s Frequency, transverse velocity v/s Frequency at node 30, 20 due to high-frequency pulse in the transverse direction at node 30, the load time history, frequency spectrum is shown in the inset image of each plot.

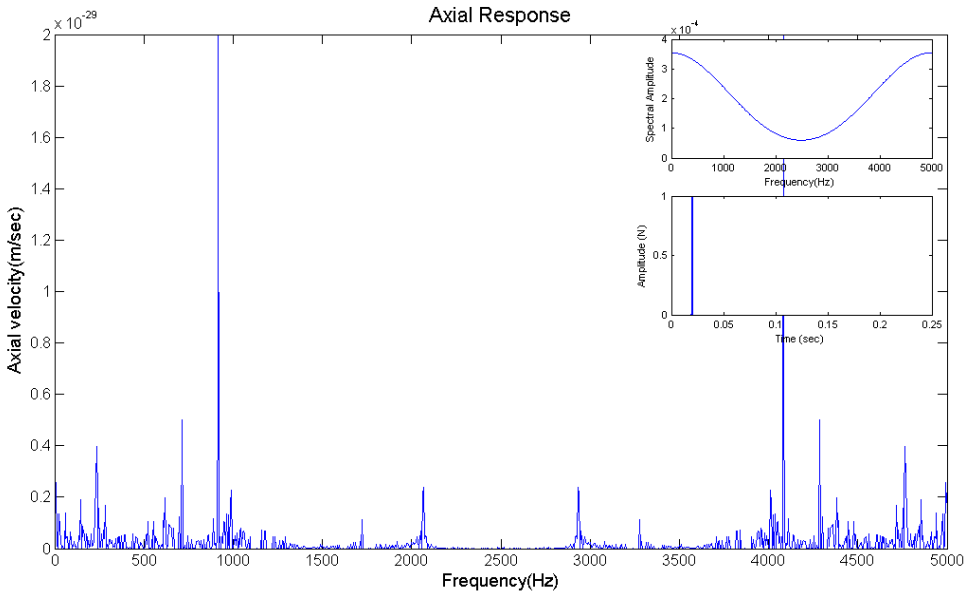

Figure 5-35 Axial velocity v/s Frequency at node 30 due to the loading (inset of the plot) in the Transverse direction.

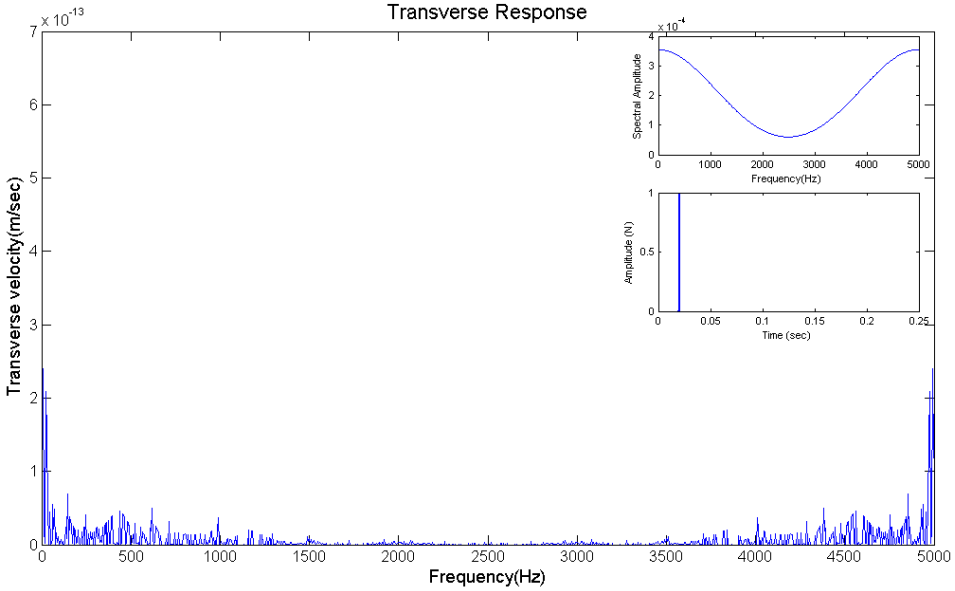

Figure 5-36 Transverse velocity v/s Frequency at node 30 due to the loading (inset of the plot) in the Transverse direction.

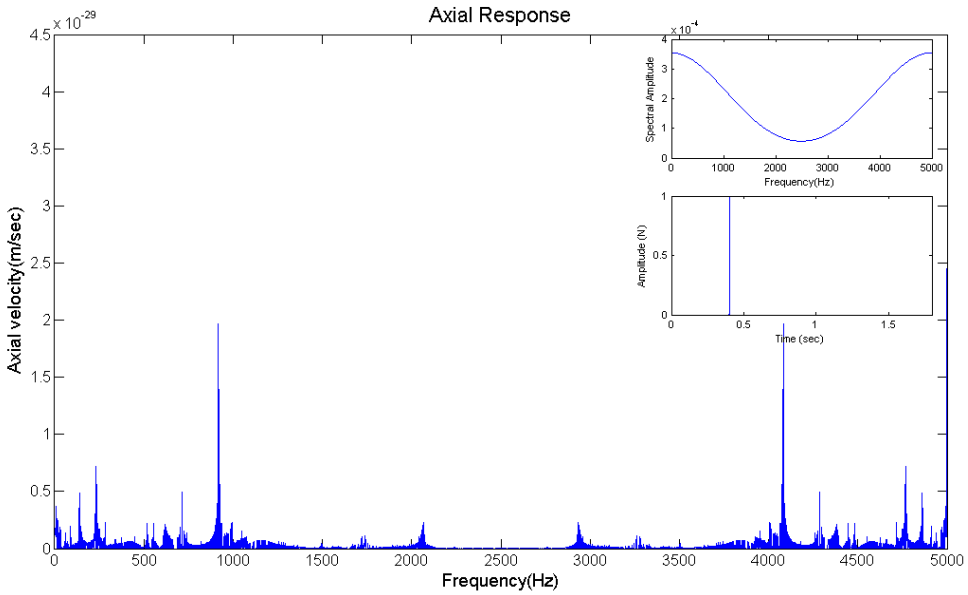

Figure 5-37 Axial velocity v/s Frequency at node 30 due to the loading in (inset of the plot) in the Transverse direction.

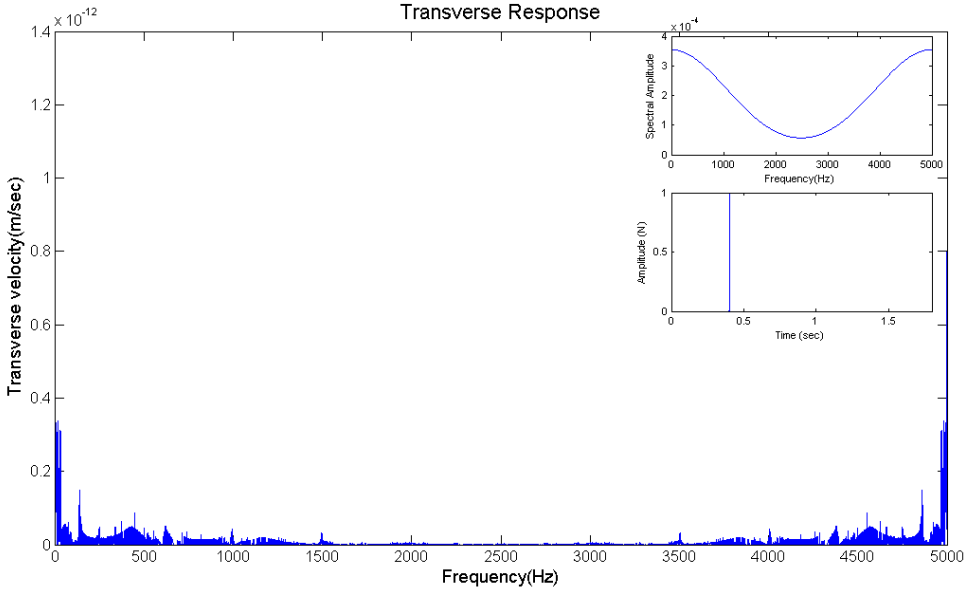

Figure 5-38 Transverse velocity v/s Frequency at node 30 due to the loading (inset of the plot) in the Transverse direction.

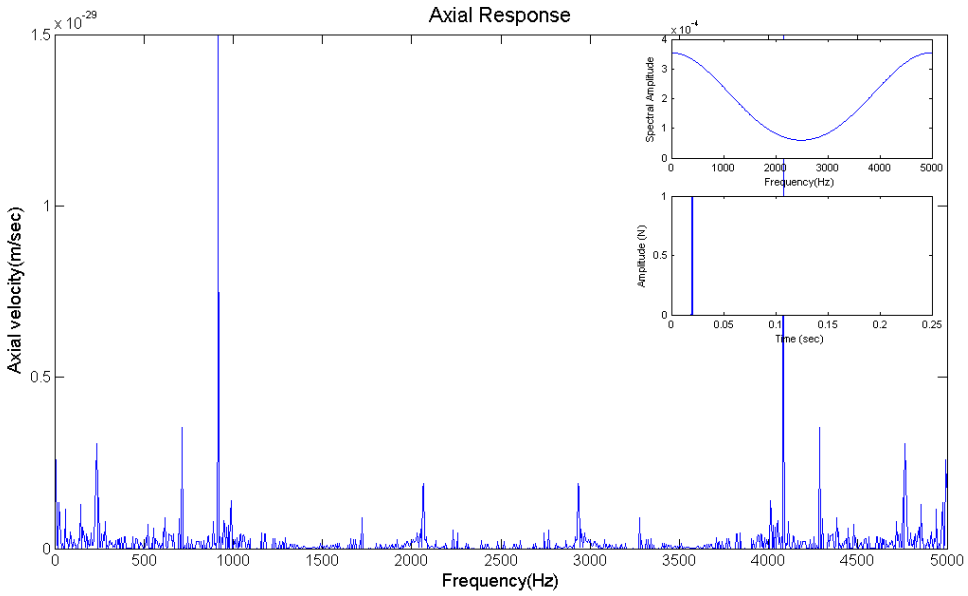

Figure 5-39 Axial velocity v/s Frequency at node 20 due to the loading (inset of the plot) in the Transverse direction.

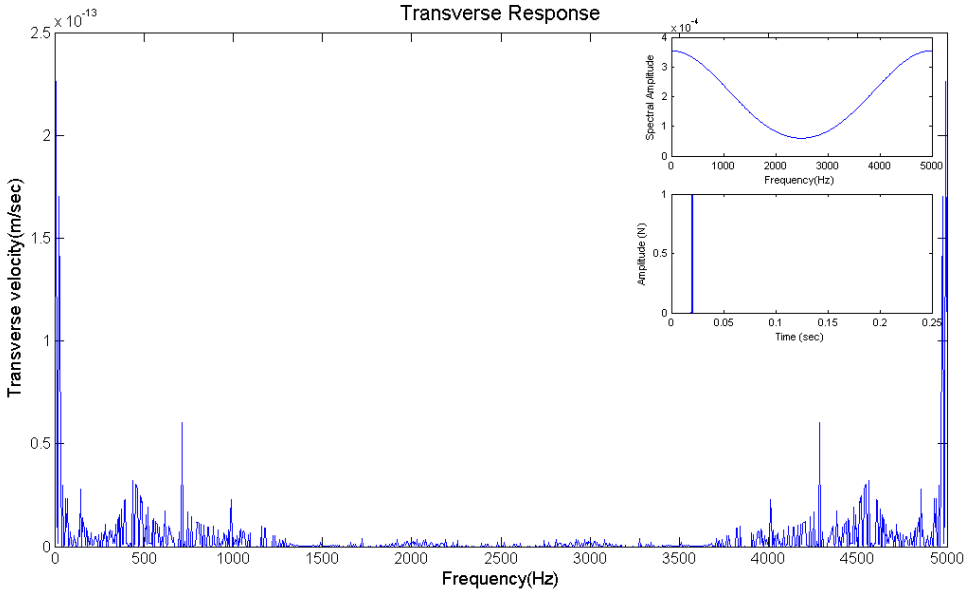

Figure 5-40 Transverse velocity v/s Frequency at node 20 due to the loading (inset of the plot) in the Transverse direction.

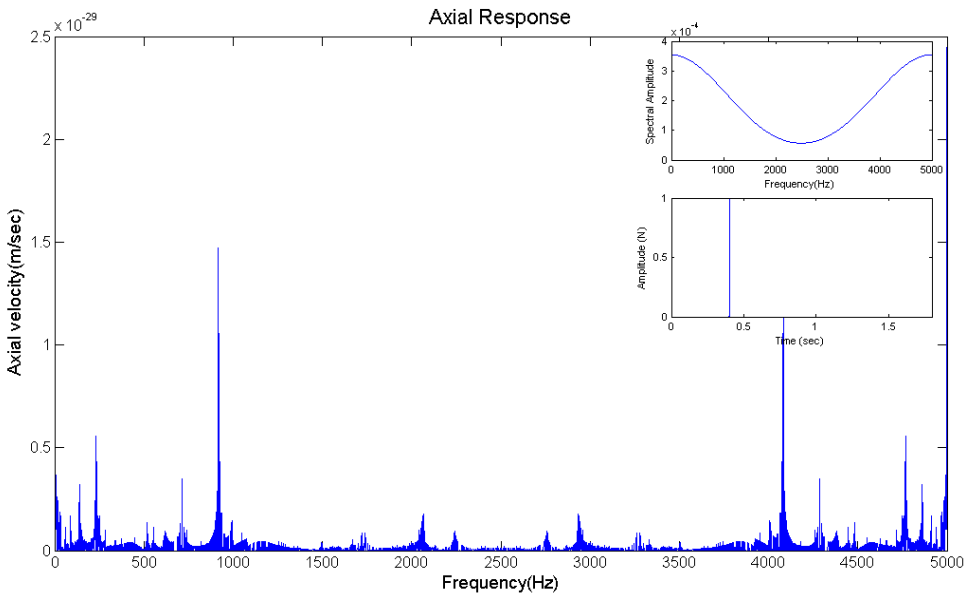

Figure 5-41 Axial velocity v/s Frequency at node 20 due to the loading (inset of the plot) in the Transverse direction.

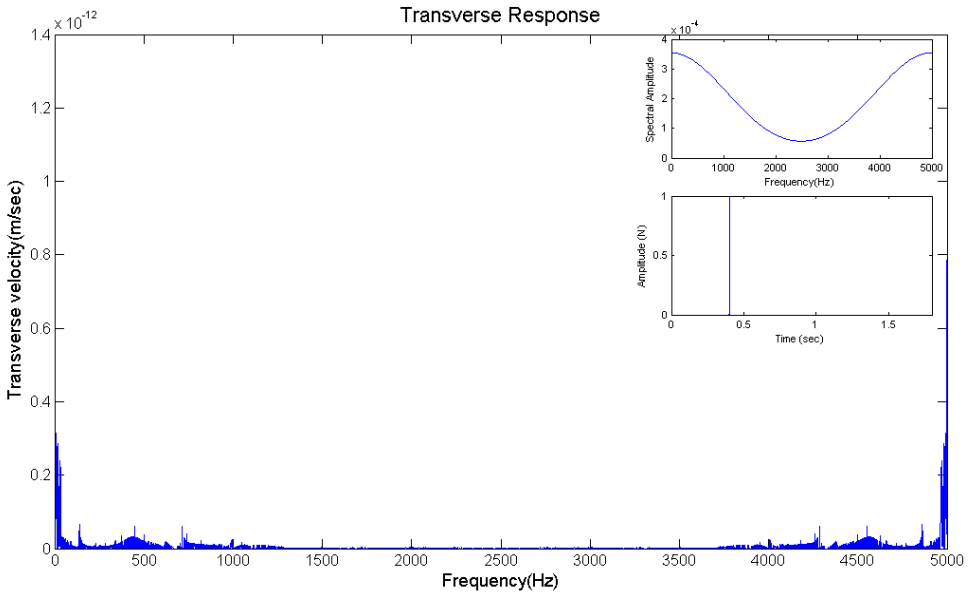

Figure 5-42 Transverse velocity v/s Frequency at node 20 due to the loading (inset of the plot) in the Transverse direction.

The following plots show a comparison of four cases Here first is healthy case, other three cases degradation of the stiffness matrix of the distributed

spring is considered with steps of 0.94, 0.88 and 0.81 at spring no.10 respectively

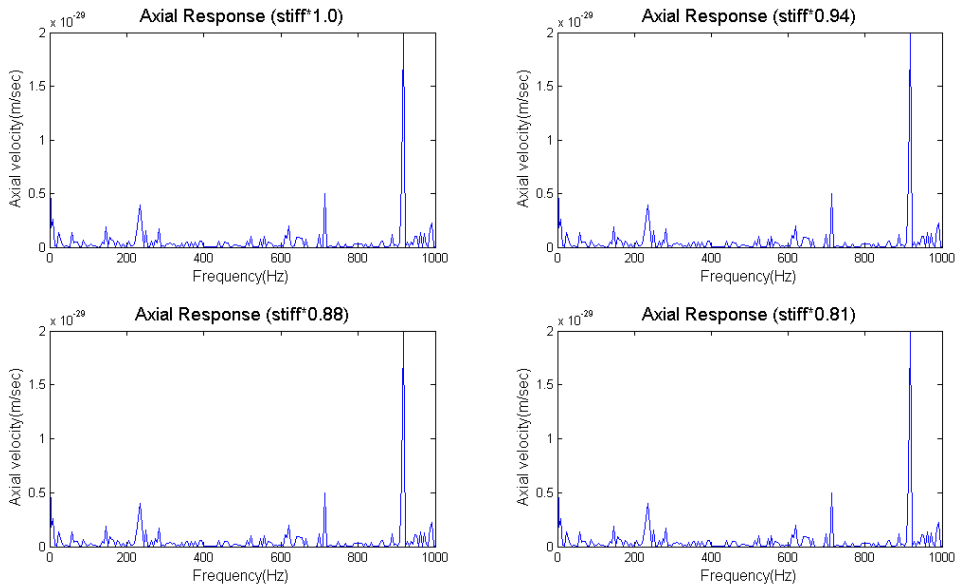

Figure 5-43 Axial velocity v/s Frequency at node 30 due to the Gaussian pulse-1.

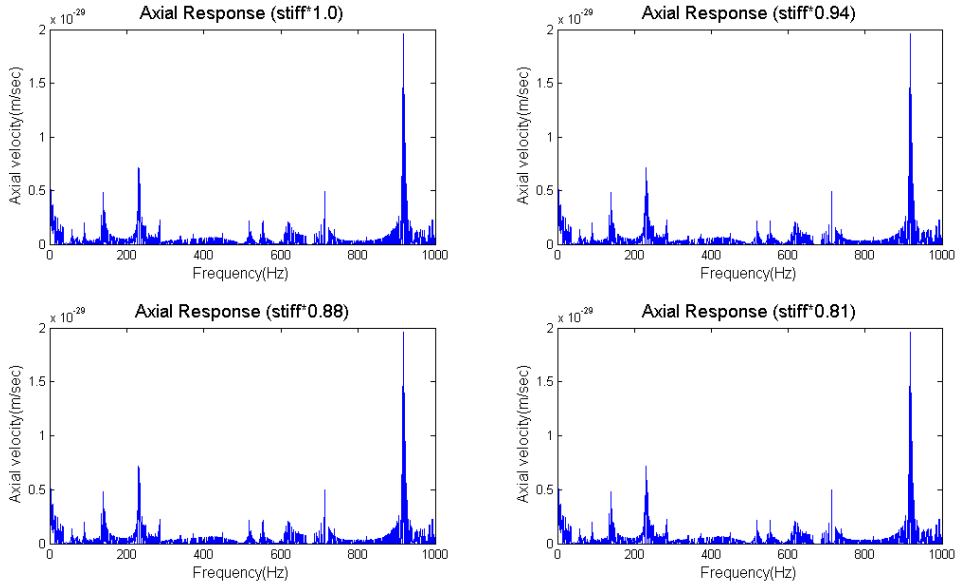

Figure 5-44 Axial velocity v/s Frequency at node 30 due to the Gaussian pulse-2.

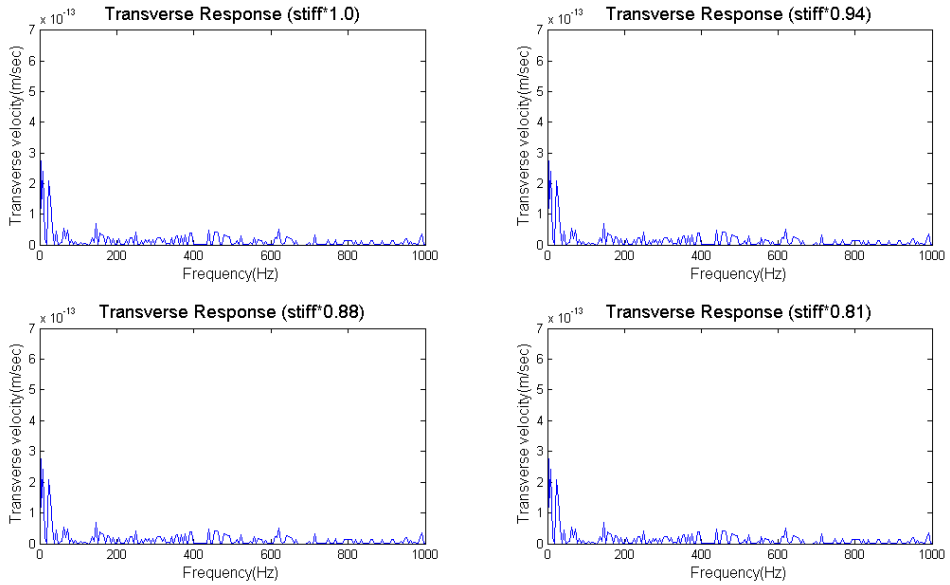

Figure 5-45 Transverse velocity v/s Frequency at node 30 due to the Gaussian pulse-1.

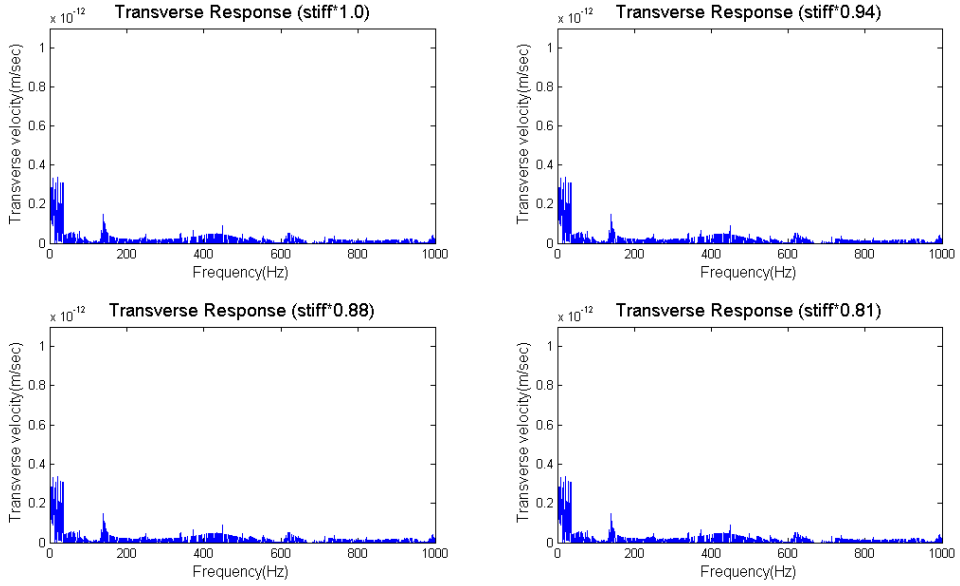

Figure 5-46 Transverse velocity v/s Frequency at node 30 due to the Gaussian pulse-2.

Chapter 6

Conclusion and Future Scope of Work

The frequency response analysis is performed for 2D Beam-Frame model of aircraft wing, for the low-high frequency loading the response is measured at all the other nodal points. The degradation in one of the distributed spring is introduced with three different steps and it is compared with the healthy case.

The spectral finite element modeling and computation reported here are aimed at the off-line computation, in which the reduced order dynamic stiffness matrix of the healthy structure is obtained and stored in the computer memory.

In the future scope of work, a near real time scenario with successive data acquisition from a sensor network and computation of DFI vector. In reality, the successive data acquisition from the sensor network and its synchronization with the computation time to obtain DFI is important, especially for damage growth monitoring.

The DFI approach we can pose it as a forward problem with a more or less global measurement and estimate the damage size. If this can be achieved in the future experimental demonstration, then it would be possible to reach the level-III SHM capability using the DFI approach.

Chapter 7

References

[1] J. Doyle, Wave Propagation in Structures, New York, 1997.

[2] S. Gopalakrishnan, A. Chakraborty, D. Roy Mahapatra, Spectral finite element method- Wave Propagation, Diagnostics and control in anisotropic and Inhomogenous Structures. Springer-verlag, London. 2008.

[3] D. Roy Mahapatra, S.Gopalakrishnan, N. Hu, Specral Finite Element Modelling of Complex Structures for Applications in Real-time Structural Health Monitoring, AIAA.

[4] D. Kumar, D. R. Mahapatra, S. Gopalakrishnan, A Spectral finite element for wave propagation and structural diagnostics analysis of composite beam with transverse crack, Finite Elements in analysis and Design 40(13-14) (2004).

[5] A. Nag, D. Mahapatra, S. Gopalakrishnan, Identifiction of delamination in a composite beam using a damaged spectral element, Structural Health Monitoring 1(1) (2002) 105-126.

[6] A. K. Garg, D. Roy Mahapatra, D. Suresh, S. Golpalakrishnan, S. N. Omkar, Estimation of composite damage model parameters using spectral finite lement method and neural network, Composite Science and Technology, 64 (2004) 2477-2493.

[7] D. Roy Mahapatra, S. Suresh, S. N. Omkar, S. Goplakrishnan, Estimation of degraded composite laminate properties using acoustic wave propagation model and a reduction-prediction network, composite laminate properties, 22 (2005) 849-876.

[8] D.S. Kumar, D. Roy Mahapatra, and S. Gopalakrishnan, Estimation of dynamic fracture parameters in a transverse cracked composite beam using a simplified diagnostic wave propagation model, Structural Health Monitoring, 2005

[9] A. K. Rao, D. P. K. Muthukumaraswamy, D. Roy. Mahapatra, S. Gopalakrishnan, and M.S. Bhat, Experimental studies toward to the development of a structural health monitoring system using damage force indicator, *Proc. Int. Conf. Smart Materials and Structures*, 2005.

[10] C.V.S. Sastry, D. Roy Mahapatra, S. Gopalakrishnan *, T.S. Ramamurthy, An iterative system equivalent reduction expansion process for extraction of high frequency response from reduced order finite element model, Comput. Methods Appl. Mech. Engg. 192 (2003) 1821–1840

[11] Usik Lee, Joohong Kim, and Andrew Y. T. Leung, The Spectral Element Method in Structural Dynamics, The Shock and Vibration Digest, 32(2000) 451-465.

[12] C T sun, Mechanics of Aircraft Structures, wiley, 2006.

[13] Component design handbook of aeronautics no.2 , London, sir Isaac pitman and sons ltd.

[14] P. Kudela, M. Krawczuk, W. Ostachowicz, Wave propagation modeling in 1D structures using spectral finite elements, journal of sound and Vibration, 300 (2007) 88-100.

[15] Arkadiusz Zak, Marek Krawczuk, Wieslaw Ostachowicz, Propagation of in-plane waves in an isotropic panel with a crack, Finite Elements in Analysis and Design, 42 (2006) 929-941.

[16] B C Lee, W J Staszewski, Modelling of Lamb waves for damage detection in metallic structures: Part I. Wave propagation, Smart Mater. Struct. 12 (2003) 804-814.

[17] Elias G, Abu-Saba, Ji Yao Shen, William M. Mcginley, Lumped mass Modelling For the Dynamic Analysis of Aircraft structures, The Journal of Aerospace Engineering.

[18] Nicole Apetre, Massimo Ruzzene, Sathyanaraya Hanagud, S. Gopalakrishnan, A Wave-Based Damage Index for the Analysis of the Filtered Response of Damaged Beams, Journal of Mechanics of Materials and Structures, 3 (2008) 1605-1623.

[19] A.K. Noor, Recent advances and application of reduction methods, Appl. Mech. Rev., Trans. ASME 47 (5) (1994) 125–146.

[20] P.Th.L.M. Van Woerkom, Mathematical models of flexible spacecraft dynamics: A survey of order reduction approaches, Control Theory Adv. Technol. 4 (1990) 609–632.